ARTICLES
https://doi.org/10.1038/s41587-022-01211-7

nature biotechnology

A comparison of experimental assays and analytical methods for genome-wide identification of active enhancers

Li Yao[1,2], Jin Liang[2], Abdullah Ozer[3], Alden King-Yung Leung[1,2], John T. Lis[1,3] ✉ and Haiyuan Yu[1,2] ✉

Mounting evidence supports the idea that transcriptional patterns serve as more specific identifiers of active enhancers than histone marks; however, the optimal strategy to identify active enhancers both experimentally and computationally has not been determined. Here, we compared 13 genome-wide RNA sequencing (RNA-seq) assays in K562 cells and show that nuclear run-on followed by cap-selection assay (GRO/PRO-cap) has advantages in enhancer RNA detection and active enhancer identification. We also introduce a tool, peak identifier for nascent transcript starts (PINTS), to identify active promoters and enhancers genome wide and pinpoint the precise location of 5′ transcription start sites. Finally, we compiled a comprehensive enhancer candidate compendium based on the detected enhancer RNA (eRNA) transcription start sites (TSSs) available in 120 cell and tissue types, which can be accessed at https://pints.yulab.org. With knowledge of the best available assays and pipelines, this large-scale annotation of candidate enhancers will pave the way for selection and characterization of their functions in a time- and labor-efficient manner.

Regulation of transcription is a synergetic process requiring both trans-regulatory factors, such as transcription factors, and cis-regulatory elements, like promoters and enhancers. In contrast to promoters, which initiate transcription in their proximal regions to produce stable RNA products, enhancers regulate their target gene(s) distally. Certain epigenomic signatures (enrichment of H3K4me1 and H3K27ac, high chromatin accessibility and CBP/p300 binding) are considered to be defining features of active enhancer loci[1,2]. However, studies also reveal that enhancers could themselves produce relatively short-lived divergent transcripts, called eRNAs[3,4]. More recent studies further showed that distal divergent transcription events are more reliable marks for active enhancers than epigenomic signatures[5,6]. Recently we proposed[7,8]—and later experimentally verified[6]—the basic unit of active enhancers that are defined by the TSSs of the divergent eRNA transcription and are delimited by the promoter-proximal RNA polymerase II (Pol II) pause sites flanking these TSSs. Therefore, to identify active enhancers genome wide it is critical to detect eRNAs and their TSSs with high sensitivity and specificity.

Enhancer RNAs are usually in extremely low abundance in cells due to their short half-life. Therefore, conventional RNA-seq experiments capture eRNAs with very low efficiency[3]. Recently, two categories of genome-wide RNA-seq assay have been developed, focusing on either TSSs or the actively transcribing polymerase positions (Fig. 1a). We named eight assays (GRO[9]/PRO-cap[10], CoPRO[8], Start-seq[11], CAGE[12], RAMPAGE[13], NET-CAGE[14], csRNA-seq[15] and STRIPE-seq[16]) from the former category as TSS assays, because these assays enrich for active 5′ TSSs of promoters and enhancers (Fig. 1a). We also named five assays (GRO-seq[17], PRO-seq[10], mNET-seq[18], Bru-seq[19] and BruUV-seq[20]) from the latter category as nascent transcript (NT) assays, because they are designed to trace the elongation or pause status of polymerases and capture their products (Fig. 1a). To enrich for RNA populations of interest these assays implement various experimental strategies, including nuclei/chromatin isolation[8–11,18], nuclear run-on[8–10] and metabolic labeling[19,20] with biotin- or bromo-tagged nucleotides and affinity purification, Pol II immunoprecipitation[18], size selection[15,16] and enzymatic elimination of non-capped RNAs[8–10,16], or chemical tagging of capped RNAs[12–14]. We summarize the key experimental steps of both TSS and NT assays in Fig. 1b. In fact, the list of all assays compared here, plus total RNA-seq[21,22], have all been used in some capacity to identify enhancer elements. However, considering that most of these assays are not specifically designed to capture eRNAs, caution should be exercised when exploiting these assays and their data to identify active enhancers.

Because these assays were initially designed for different purposes, various computational tools were developed for exploring and interpreting the raw experimental data—for example, Tfit[23], dREG[24,25] and dREG.HD[26] were developed to identify transcriptional regulatory elements (TREs) from some NT assays, including GRO-seq and PRO-seq; FivePrime[27] (based on paraclu[28]), GROcapTSSHMM[7] and HOMER[15] were introduced for analysis of data from CAGE, GRO-cap and csRNA-seq, respectively. While all these tools can potentially be used to identify eRNA transcription and active enhancers, there has not been a systematic evaluation and comparison of their performance with datasets generated by the aforementioned experimental assays.

In this study we systematically examined 13 experimental assays, including seven TSS assays, five NT assays and total RNA-seq (as the outgroup), in terms of their sensitivity and specificity for capturing eRNAs. We also developed a computational tool, PINTS, which is designed to identify enhancer candidates from these assays. Moreover, by comparison of PINTS with eight other widely used computational tools, we found that PINTS gave the highest

[1]Department of Computational Biology, Cornell University, Ithaca, NY, USA. [2]Weill Institute for Cell and Molecular Biology, Cornell University, Ithaca, NY, USA. [3]Department of Molecular Biology and Genetics, Cornell University, Ithaca, NY, USA. ✉e-mail: jonhlis@cornell.edu; haiyuan.yu@cornell.edu

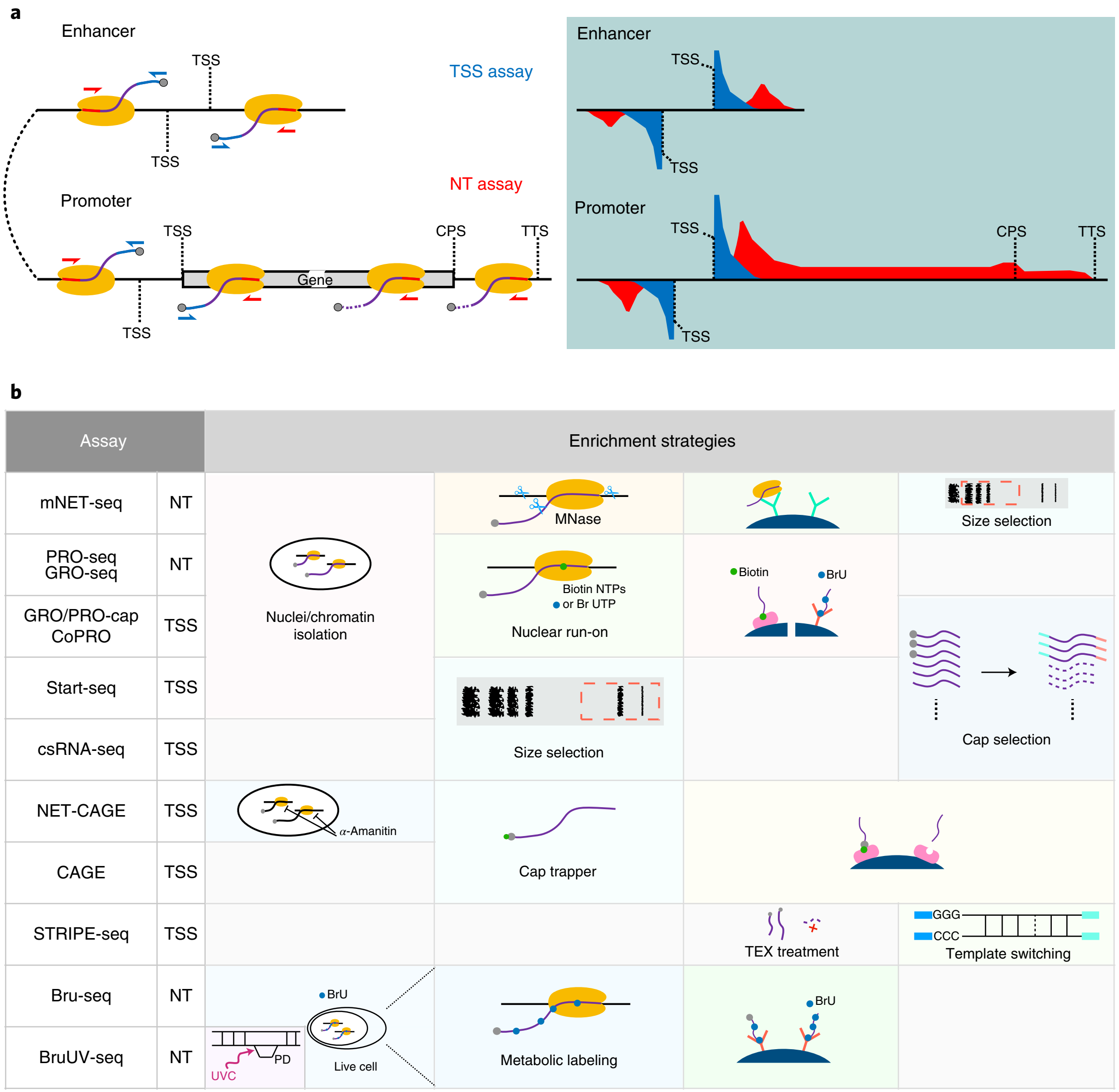

Fig. 1 | Comparison of currently available assays for detection of eRNAs. a, Schematics of enhancer and promoter/gene transcription by RNA Pol II (left) and characteristic profiles of TSS and NT assays (right, area shaded light blue). Black lines represent genomic DNA; nascent RNAs are denoted by purple curved lines with 5′ and 3′ ends colored blue and red, respectively, and gray spheres as caps and yellow ovals indicating RNA Pol IIs. Arrows indicate the direction of sequencing reads, TSS assay in blue and NT assay in red. Representative read density profiles are colored blue or red for TSS and NT assays, respectively. CPS, cleavage polyadenylation site; TTS, transcription termination site. **b**, Enrichment strategies used in different TSS and NT assays. TEX, terminator exonuclease; UVC, ultraviolet C; PD, pyrimidine dimer. A detailed description is available in Supplementary Notes.

overall performance pertaining to robustness, sensitivity and specificity, especially when analyzing data from TSS assays. Finally, we constructed a comprehensive enhancer candidate compendium for 120 cells and tissues using the robust and unified definition of active enhancers based on detected eRNA TSSs genome wide[5–7], and developed an online web server (https://pints.yulab.org/) to navigate, prioritize and analyze enhancers based on a wide range of genomic and epigenomic annotations. We expect that our enhancer compendium will become a valuable resource to the research community for the effective selection of candidate enhancers for further functional characterization.

Results

TSS assays are more sensitive in regard to eRNA detection. To perform a quantitative comparison of eRNA detection sensitivity, we first normalized all libraries by downsampling them to the same sequencing depth as the library with the lowest depth (18.9 million mappable reads; Supplementary Table 1). We then compared the assays' sensitivity by examining their coverage in 803 (635 intergenic, 113 intronic and 55 others) previously identified bona fide enhancers validated by CRISPR–Cas9-mediated deletion and CRISPR interference (CRISPRi) in K562 cells[29–37] (CRISPR-identified enhancer set, Methods and Supplementary Table 2). With the same sequencing depth, GRO-cap ranks first in sensitivity: it covers 86.6% of CRISPR-identified enhancers (70.4% divergent: ≥five reads detected from both strands, and 16.2% unidirectional: ≥five reads detected only on one strand; Fig. 2a and top track in Extended Data Fig. 1a). csRNA-seq is in second place, with 73.7% (47.3% divergent and 26.4% unidirectional) coverage of these validated enhancers (Fig. 2a and Extended Data Fig. 1a). We re-evaluated the sensitivity of the 13 assays using another set of reference enhancers (previously validated by massively parallel reporter assay (MPRA)[38–42] and self-transcribing active regulatory region sequencing (STARR-seq)[6,43–45]), and the results remained the same (Extended Data Fig. 1a, bottom). Furthermore, to test the robustness of our conclusion, we also evaluated the sensitivity

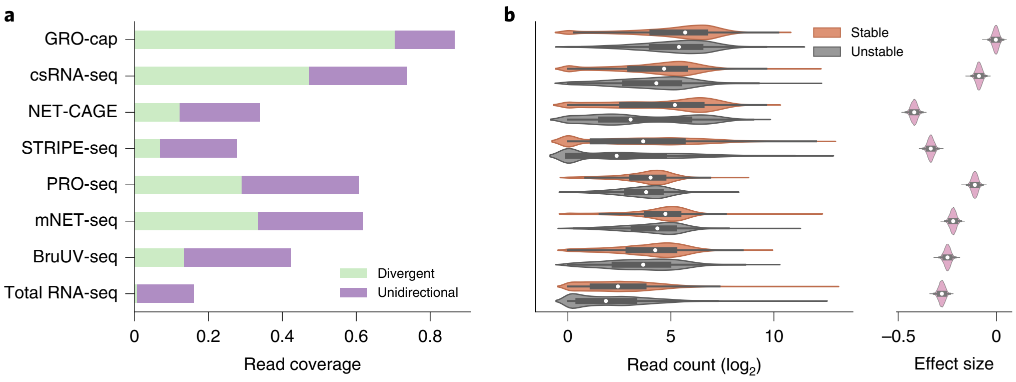

Fig. 2 | Evaluation of assay sensitivity in eRNA detection. a, The capability of different assays to capture validated enhancers (CRISPR-identified enhancer set). All libraries were downsampled to the same sequencing depth. Unidirectional and divergent indicate the detection of eRNAs originating from either one or both strands of the enhancer loci, respectively. **b**, Differences in read coverage among stable ($n=13,861$) and unstable ($n=6,380$) transcripts. GRO-cap showed the highest coverage of both stable and unstable transcripts and the least preference toward stable transcripts. Preferences (effect sizes) were evaluated as Cohen's *d* via bootstrap ($n=5,000$). In the box plot the center dots, box limits and whiskers denote the median, upper and lower quartiles and 1.5× IQR, respectively.

of eight assays with data available for another cell line, GM12878, using STARR-seq-identified enhancers as reference[6,46]. As with K562 (Extended Data Fig. 1a), GRO-cap was the most sensitive assay for detection of active enhancers in GM12878 (Extended Data Fig. 1b).

We further evaluated the sensitivity of these assays by their ability to capture unstable transcripts. eRNAs are usually less stable than messenger RNAs, and this was the case seen here by comparing decay rates of transcripts[47] from 514 CRISPR-identified enhancers to mRNAs (*P* value from two-sided Mann–Whitney *U*-test $<10^{-10}$; rank-biserial correlation, 0.442). We then used as the cutoff between stable and unstable transcripts the 95th quantile of decay rates of mRNAs and surveyed the distribution of read counts captured in the two categories among all assays. Consistent with our conclusion above, GRO-cap showed the smallest differences in read coverage between stable and unstable transcripts (Cohen's *d*, −0.003; 95% confidence interval (CI) (−0.033, 0.023)), indicating that assays using nuclear run-on followed by cap selection have the greatest ability to enrich unstable transcripts, which is of particular importance in detection of eRNAs (Fig. 2b and Extended Data Fig. 1c). We evaluated the effects of technical artifacts, including strand specificity and mispriming, and our results suggest that all libraries have high strand specificity (average, 0.984; s.d., 0.019; Extended Data Fig. 2a–c) and low internal priming rates (Supplementary Notes and Extended Data Fig. 2d,e).

Cap selection or Pol II pausing does not bias eRNA capture. Assays enriching for capped RNAs showed an advantage in detection of eRNAs (Fig. 2a,b). Because not all eRNAs are necessarily capped, we wanted to assess whether the fraction of capped eRNAs would influence these quantifications of eRNAs. To address this concern we reanalyzed a previously published dataset[6], where libraries were prepared with input RNAs preselected for different capping states (capped, uncapped and unselected), and we assessed the abilities of these libraries to detect CRISPR-identified enhancers. The difference among libraries prepared with three different inputs is minimal: there is a ~97% overlap between the library prepared with capped RNAs and that with unselected RNAs. Therefore, we consider the bias in enhancer detection as negligible when enriching for capped RNAs (Extended Data Fig. 2f,g and Supplementary Notes).

Another concern about run-on assays is whether paused polymerases can efficiently resume elongation. A previous study in *Drosophila* showed that sarkosyl treatment could unleash paused polymerases and allow for efficient elongation of nascent RNAs that correlated with Pol II levels as measured by chromatin immunoprecipitation sequencing (ChIP–seq)[48]. Here, we calculated the correlation coefficient of promoter reads detected by PRO-seq and POLR2A ChIP-exo[49] associated with paused Pol IIs in human K562 cells and found little difference, indicating that paused Pol IIs elongate efficiently in run-on assays (Extended Data Fig. 2h).

Gene body reads in NT assays contribute to lower sensitivity. For the two families of assays that we compared in this study, we noticed that TSS assays are generally more sensitive in detection of eRNAs than NT assays, even for assays that use very similar enrichment strategies (Fig. 1b). For instance, while both GRO-cap and PRO-seq employ similar nuclear run-on procedures, there is a 41.3% difference between their divergent coverage of the CRISPR-identified enhancer set (Fig. 2a). When inspecting the genome-wide distribution of reads (Fig. 3a and Extended Data Fig. 3a), we noticed that NT assays have significantly higher proportions of reads arising from gene body regions (mean of NT assays, 65.6%; mean of TSS assays, 13.0%; *P* value derived from two-sided Mann–Whitney *U*-test, 0.003), which is not surprising as they are designed to reveal all actively transcribing RNA polymerases whereas TSS assays are specifically designed to identify TSSs. Because eRNA transcription is, on average, much lower than that of genes[7], such a high portion of gene body reads in NT assays dilutes the signal from eRNAs and substantially lowers their sensitivity in regard to detection of active enhancers. As shown in Fig. 3b, NT assays detect a substantial number of reads in the *FAM89A* gene body whereas TSS assays have reads in only the promoter regions of the *FAM89A* gene. As a result, almost all NT assays (except PRO-seq) have no discernable signal at a distal enhancer locus near the *FAM89A* gene that was validated by CRISPRi[34] (Fig. 3b). Another potential problem regarding NT assays is that reads that are mapped to intergenic or intronic regions could be derived from either eRNAs, the unprocessed precursors of RNAs from other categories (for example, pre-mRNAs) or read-through from an upstream transcription event (Extended Data Fig. 3b), which further reduces their sensitivity in detection of eRNAs.

Most RNA transcripts in living cells belong to the families of highly abundant RNAs—for example, ribosomal RNAs and small nuclear RNAs. When capturing eRNAs with sequencing-based methods, a successful exclusion of RNAs of these high-abundance families from the sequencing libraries during the preparation process can greatly enhance the efficiency and sensitivity of eRNA identification. We compiled a comprehensive list of high-abundance RNAs

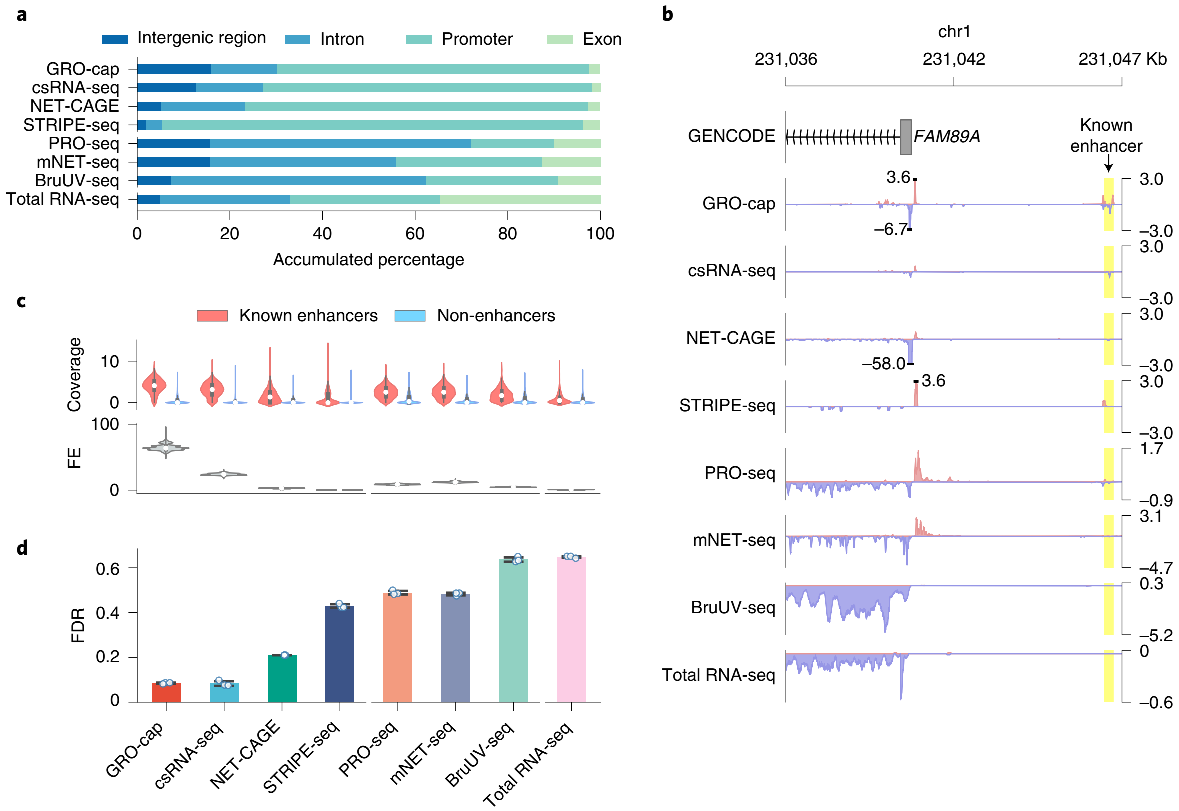

Fig. 3 | Characterization of factors affecting assay sensitivity and evaluation of assay specificity in eRNA detection. a, Genome-wide distribution of sequencing reads originating from intergenic regions, introns, exons and promoters detected by different assays. **b**, Genome browser snapshot of a gene (*FAM89A*) and its enhancer (highlighted in yellow) demonstrating the different patterns of signals captured by TSS (enriched in the promoter and enhancer regions) versus NT (enriched in the promoter and gene body regions) assays. Signals are normalized by RPM. **c**, Specificity in detection of eRNAs. Top: differences in read coverage among CRISPR-identified enhancer ($n=803$) and non-enhancer ($n=6,777$) loci; a pseudocount (1) was added to each locus and the coverage was log transformed. Bottom: signal-to-noise ratios depicted in terms of fold enrichment (FE); results are based on bootstrapped samples ($n=10,000$), and median statistics are used to calculate fold changes. In the box plot the center dots, box limits and whiskers denote the median, upper and lower quartiles and 1.5× IQR, respectively. **d**, FDRs estimated by overlap between the top 20,000 genomic bins and the reference (803 CRISPR-identified and 6,777 non-enhancer) loci. Downsampled libraries were used ($n=3$); values and error bars represent mean and s.d.

in human cells by incorporating annotations from GENCODE[50], RefSeq[51] and RMSK[52]. Based on this list, an average of 7.12% of the mappable reads in each assay originated from rRNAs despite most of the assays employing strategies to reduce rRNA inclusion (Extended Data Fig. 3c). By simulating an rRNA-depleted BruUV-seq library, we found that complete depletion of rRNAs could contribute to a 1.76-fold boost in detection of eRNAs (Extended Data Fig. 3d).

When the assay specifically enriches for short transcripts, like csRNA-seq, a relatively large proportion (31.5%) of mappable reads were found to have originated from snRNAs (Extended Data Fig. 3c). Detection of such a disproportionally large fraction of snRNAs suggests potential contamination in the sequencing library from the splicing intermediates. To test this possibility, we calculated signal density at all splice sites in the human genome according to GENCODE annotation (release 24, comprehensive version)[50]. As shown in Extended Data Fig. 3e, csRNA-seq detected more signals at the splicing junctions than all the other assays.

TSS assays, especially GRO-cap, have higher specificity. While genomic regions with detectable transcriptional events account for 75% of the human genome[53], many of these events are considered to be spurious transcriptional noise[54,55] because of their extremely low transcript yields compared to mRNAs and the intrinsic promiscuity of RNA Pol II under certain circumstances[56]. Therefore, it is critical to detect and differentiate reads that originated from spurious transcription in these assays. To that end, we collected non-enhancer loci from eight MPRA[38–42] and STARR-seq[6,43,44] studies and further removed elements overlapping with predicted enhancer-like sequence (ELS) or promoter-like sequence (PLS) from candidate cis-regulatory elements (cCRE) annotations[57] to generate a set of 7,097 loci (referred to as the ‘non-enhancer set’; Methods, Extended Data Fig. 4a and Supplementary Table 3). We observed that signal intensities in the CRISPR-identified enhancer set are often higher than those in the non-enhancer set (Fig. 3c and Extended Data Fig. 4b; all with *P* values from two-sided Mann–Whitney *U*-test $<10^{-10}$), with GRO-cap having the highest signal-to-noise ratio (64-fold enrichment; Fig. 3c and Extended Data Fig. 4b for K562 and Extended Data Fig. 4c for GM12878).

We also calculated the false discovery rate (FDR) for each assay based on the overlap of their reads with both the CRISPR-identified enhancer and non-enhancer sets. We found that TSS assays generally have lower FDR than NT assays (TSS assay mean, 0.232 versus NT assay mean, 0.544; *P* value from two-sided Mann–Whitney *U*-test 2.0×10^{-5}; Fig. 3d and Extended Data Fig. 4d), with assays enriching for capped and short RNAs having the lowest FDR (mean, 0.083; s.d., 0.007).

PINTS. Two categories of tools are currently available to process data generated by RNA-seq assays. Tools in the first category predict entire transcription units and are primarily used for NT assays, for example, HOMER (GRO-seq)[58] and groHMM[59], to determine the start and end positions of transcription units (Extended Data Fig. 5a). Tools in the second category usually identify narrower regions for potential regulatory elements (mainly promoters and enhancers, often referred to as peak callers) and include GROcapTSSHMM[7], dREG[24], Tfit[23], dREG.HD[26], TSScall[11], HOMER (csRNA-seq)[15] and FivePrime[27] (based on Paraclu[28]). Based on previous studies, the peak of divergent TSSs, which is associated with eRNA transcription, is an effective mark for active enhancers[5,6]. Therefore, in this comparative study, we focused on the second category of computational tools.

To achieve higher resolution in identification of transcriptional regulatory elements, a common practice is to look only at the ends of captured transcripts. Two critical issues emerge when evaluating the statistical significance of peaks (that is, TSSs), especially for TSS assays. First, when considering only transcript ends the fraction of zeros (no mapped reads per base pair) in the local background increases, which deflates read density in the local background and thus inflates the statistical significance of candidate TSSs and results in false positives. Second, multiple TSSs can localize in close proximity in the genome and therefore inflate the estimation of read density in the local background, resulting in diminished statistical significance for all TSSs in that locus and leading to false negatives in TSS detection. To address these issues, we developed PINTS, which uses zero-inflated Poisson models to evaluate local read densities and employs interquartile range (IQR)-based refinement to ameliorate false negatives by conditional masking of candidate TSSs in the local background (Extended Data Fig. 5b). PINTS was inspired by MACS2 (ref. [60]), with modifications specifically implemented for identification of eRNA TSSs from genome-wide TSS assays. After evaluation of the significance of each TSS, PINTS defines TREs as divergent TSS pairs that are within 300 base pairs (bp) of each other, as suggested by previous studies[6,8] (Extended Data Fig. 5b and Methods). We identified candidate enhancers as distal TREs >500 bp away from known protein-coding gene TSSs[6].

Peak callers vary in resolution and computational needs. Candidate enhancer loci identified by different algorithms should share the same features as CRISPR-identified enhancers with characteristic epigenomic marks (DHS, H3K27ac, H3K4me3 and H3K4me1) and transcription factor (CBP/p300, GATA1 and CTCF)-binding sites. Indeed, we found that candidate enhancers identified by most tools recapitulate these features of CRISPR-identified enhancers (Fig. 4a,b and Extended Data Fig. 6a). However, the patterns of epigenomic marks and transcription factor binding sites of candidate enhancers identified by MACS2 (ref. [60]), a widely used peak caller for analysis of ChIP–seq data, are distinct from those of CRISPR-identified enhancers, suggesting that the default peak-shifting model of MACS2 may not be suitable for identification of eRNA TSSs of active enhancers (Supplementary Notes and Extended Data Fig. 6b).

We further surveyed the size distribution of these elements as an indication of peak-calling resolution. We found that PINTS, GROcapTSSHMM, Tfit and TSScall achieved higher resolution (average peak size of 185–300 bp) than other tools in analysis of TSS assay data (Fig. 4c and Extended Data Fig. 6c). Notably, peaks called by dREG.HD and MACS2 ranged between 548 and 751 bp in size, whereas those of dREG, FivePrime and HOMER ranged between 381 and 460 bp.

The amount of computational resources required by a peak caller greatly affects its general applicability. Here, we compared the total amount of central processing unit (CPU) time and peak memory usage required by each tool for identification of divergent elements from TSS assays (Fig. 4d,e). Based on our calculation, it is feasible to run PINTS, MACS2, HOMER, GROcapTSSHMM, TSScall and FivePrime on a typical personal computer.

PINTS achieves high overall performance for TSS assays. A common task in functional studies of enhancers is to compare active enhancers across different conditions and diseases[21,22], which requires that in silico enhancer-predicting tools be robust against biological and experimental variances. To test the upper bound of robustness for the aforementioned tools, we performed peak calling using these tools on datasets from 12 assays by aligning each dataset to two commonly used builds of the human reference genome: hg19 and hg38. Because there is no variation in the sequencing datasets themselves and the two reference genome builds are very similar[61] (Extended Data Fig. 7a), we expected that differences in peak calls using these two different genome builds would be minimal across all datasets. We found that by simply changing the reference genome builds, half have a Jaccard index <0.9 for at least one assay (Fig. 4f). Furthermore, we noticed that Jaccard indices were even lower when we tried to evaluate robustness across real technical and biological replicates (average, 0.507; s.d., 0.246), especially for TSScall and FivePrime, where their robustness was only 0.401 (s.d., 0.104) and 0.384 (s.d., 0.203), respectively (Extended Data Fig. 7b). PINTS consistently showed a high level of robustness in both cases (average 0.976, s.d. 0.008 between genome builds; and average 0.728, s.d. 0.052 across replicates).

To evaluate sensitivity and specificity, two key performance metrics, we merged the CRISPR-identified enhancer set with the promoter regions from GENCODE v.24 (ref. [50]) as the positive set and non-enhancer loci as the negative set (Methods and Extended Data Fig. 8a). We then evaluated each tool's performance for all TSS assay datasets (Fig. 4g). The results show that PINTS achieved the best balance between sensitivity and specificity (PINTS mean area under the curve (AUC) 0.780, s.d., 0.082; mean AUC for the second-best tool (dREG) 0.652, s.d. 0.109). Moreover, when we compared the performance of all available tools on sparsely sequenced libraries (with 18.9, 15 and 10 million mappable reads), PINTS still outperformed the other tools (Extended Data Fig. 8b–d). When evaluating unique TREs identified by PINTS, we noticed enrichments in epigenomic marks (H3K27ac and H3K4me1; Extended Data Fig. 9a) and motifs for both enhancer-activity-related and cell-type-specific transcription factors (Extended Data Fig. 9b). For all of these computational tools we summarize their key requirements, main characteristics and applicability to different RNA-seq assays in Extended Data Fig. 10.

An enhancer compendium for human cell and tissue types. Previous studies have shown that, compared with histone marks, detection of enhancers by divergent eRNA TSSs has advantages in both resolution and specificity[5,6]. Introducing an eRNA-centric enhancer compendium, in addition to all available enhancer datasets based on histone marks[57,62], will be an invaluable resource to better understand gene regulation, to functionally annotate the noncoding genome and to help prioritize noncoding variants across disease cohorts by their potential impact on enhancer activities[63]. Toward this goal, we applied PINTS to identify candidate enhancers using TSS assay datasets (that is, GRO/PRO-cap, CoPRO, csRNA-seq, NET-CAGE, RAMPAGE, CAGE and STRIPE-seq) across 33 cell lines, seven in vitro differentiated cells, 35 primary cells and 45 tissue samples, including all available TSS assay datasets through the ENCODE portal (Fig. 5a). Such a comprehensive catalog of enhancers across a wide range of human cells and tissues analyzed by the same exact computational pipeline provides an excellent resource to perform meaningful comparative genomic analyses for studying the dynamics of enhancers and gene regulation in general, which will help focus on true biological differences while minimizing technical variations. In addition, for seven human cell lines (K562, GM12878, HepG2, HeLa-S3, MCF-7, H9 and HCT116) we applied all other available tools (FivePrime, HOMER, TSScall, dREG, dREG.HD and Tfit) to identify candidate enhancers. We believe that this unique

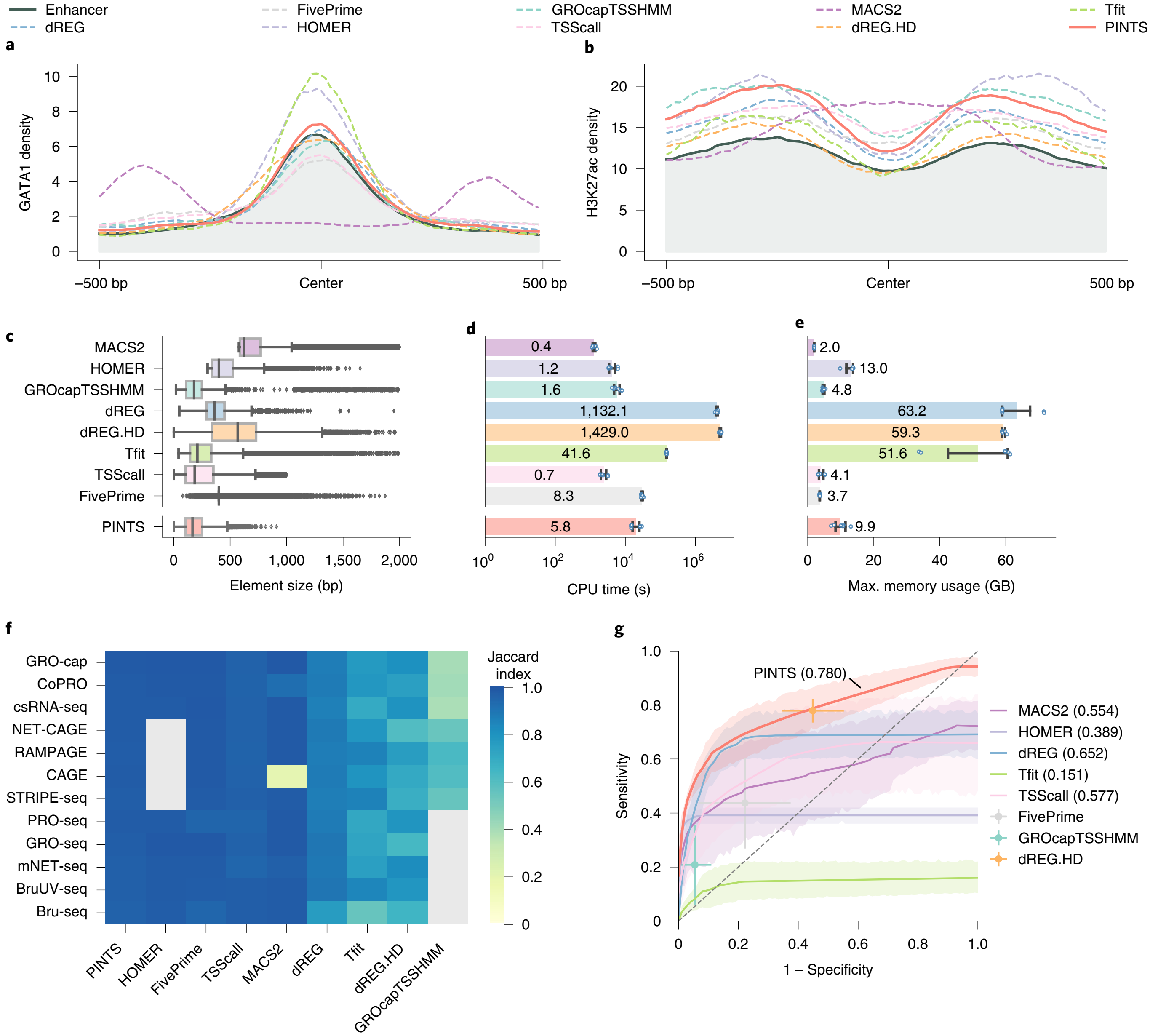

Fig. 4 | PINTS achieves optimal balance among resolution, robustness, sensitivity, specificity and computational resources required. a,**b**, Profiles of GATA1 binding sites (**a**) and H3K27ac pattern (**b**) in CRISPR-identified enhancer regions and distal TREs identified by different peak callers. **c**, Distribution of element sizes identified by different tools. Sample sizes from top to bottom: 38,703, 9,546, 19,886, 51,128, 56,300, 17,152, 54,002, 40,042, 35,998. In the box plot the center lines, box limits and whiskers denote the median, upper and lower quartiles and 1.5× IQR, respectively. Points show observations not 1.5× IQR. **d**, CPU time consumed by peak callers in identifying elements from various TSS assay libraries. The average CPU time labeled within each bar is in the unit of hours (*n* = 6). **e**, Maximum memory usage during peak calling from TSS assay libraries. The average maximum usage labeled within or above each bar is in the unit of gigabytes (*n* = 6). **d**,**e**, Values and error bars represent mean and s.d. **f**, Robustness of peak calls made by different tools. Libraries were mapped to both hg19 and hg38, and robustness was measured as the Jaccard index between calls from hg19 and hg38 (lifted over). Cells colored gray indicate either that the tool cannot be applied to the corresponding assays or that one or more required datasets are not available. **g**, Aggregated ROC curves for each peak caller on all TSS assay datasets (*n* = 7). Solid lines represent mean values and corresponding shaded areas denote 95% CI of the means (via bootstrap). For tools where ROCs cannot be calculated, solid dots represent their performance with default parameters. Values and error bars show the mean and s.d.

resource of enhancers in seven cell lines, with multiple TSS assay datasets analyzed by all available computational tools, will greatly help further studies of enhancers and their key architecture characteristics. All of these candidate enhancer calls are made publicly available through our web server (https://pints.yulab.org) and are described in detail below. We will regularly update our enhancer compendium as new datasets, especially those for new cell lines or samples, and assays become available.

In human K562 cells where datasets were available from all TSS assays, our results show that GRO-cap has by far the highest number of distal TREs (19,006 identified by PINTS, with 9,531 unique enhancer calls not identified by any other assay); the second-best

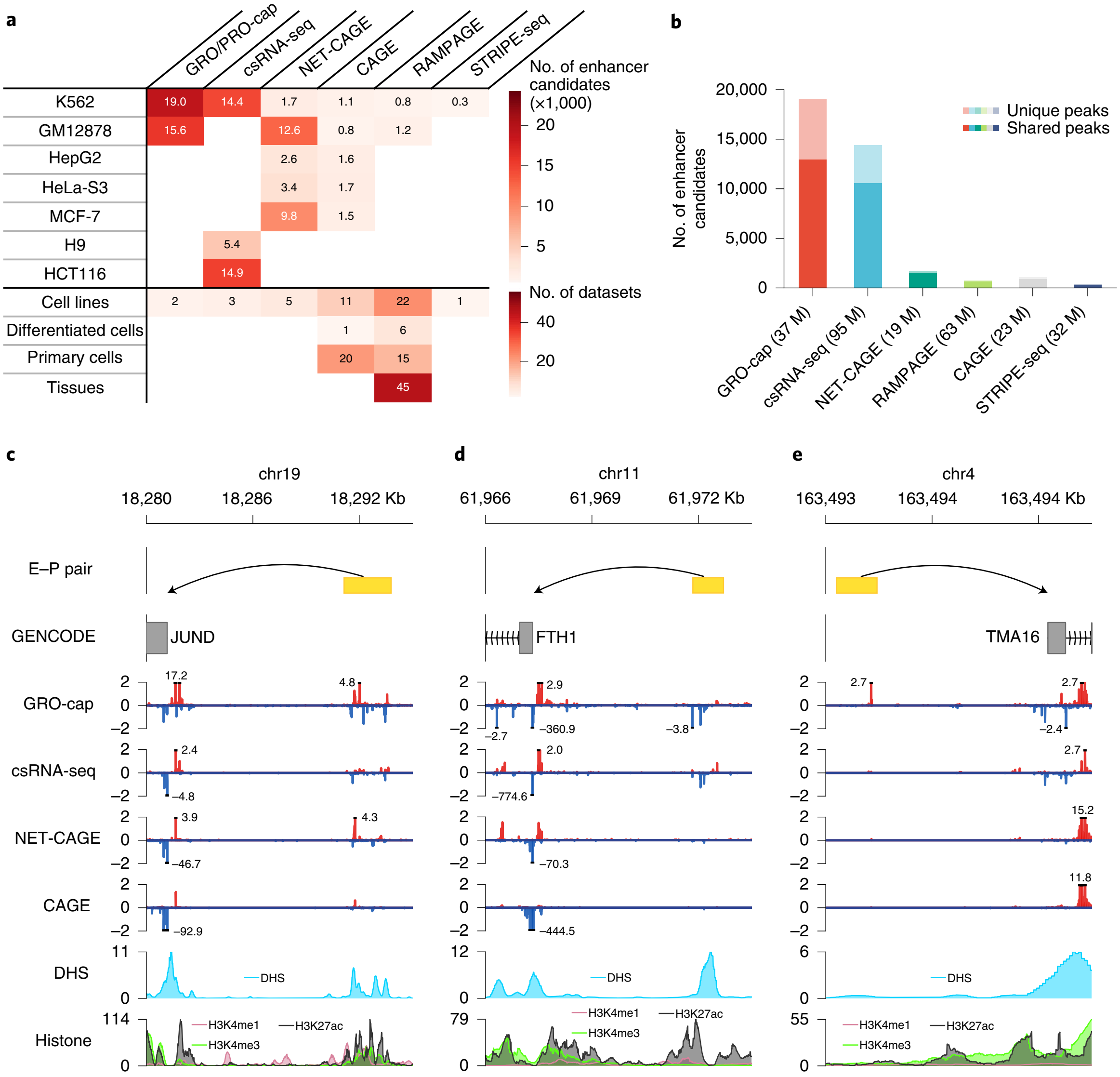

	GRO/PRO-cap	csRNA-seq	NET-CAGE	CAGE	RAMPAGE	STRIPE-seq
K562	19.0	14.4	1.7	1.1	0.8	0.3
GM12878	15.6		12.6	0.8	1.2	
HepG2			2.6	1.6		
HeLa-S3			3.4	1.7		
MCF-7			9.8	1.5		
H9		5.4				
HCT116		14.9				
Cell lines	2	3	5	11	22	1
Differentiated cells				1	6	
Primary cells				20	15	
Tissues					45	

Fig. 5 | A comprehensive human enhancer compendium. a, Summaries of all distal elements identified from different assays with PINTS in seven cell lines (top) and 131 datasets generated by different assays across 120 biosamples included in our enhancer compendium (bottom). Differentiated cells were differentiated in vitro. **b**, The number of distal elements identified by PINTS from different assays in K562. Darker shading indicates the proportion of shared elements identified from at least one other assay; lighter shading indicates elements unique to the corresponding assay. The number of mappable reads for each assay is given in parentheses. **c**, A known enhancer locus where most of these assays captured signals on both strands. **d**, A known enhancer locus where only GRO-cap and csRNA-seq captured detectable signals. **e**, A known enhancer locus where only GRO-cap captured clear signals. E-P. enhancer–promoter. **c–e**, Signal tracks were normalized by their sequencing depth (RPM).

dataset, csRNA-seq, has only 14,375 enhancer calls with 5,048 unique (Fig. 5b). This is not surprising given that GRO-cap showed the highest sensitivity in detection of eRNA transcription (Fig. 2a,b), and the GRO-cap dataset has the third-highest read depth (Fig. 5b). We selected three CRISPRi-validated enhancer–promoter pairs[34] to visualize these differences, and show the variety in signal abundance across different datasets (Fig. 5c–e). For example, the enhancer that regulates the *JUND* gene (Fig. 5c) has reasonable accessibility and is supported by epigenomic marks, including H3K27ac and H3K4me1. As expected, all four TSS assays could identify this enhancer. The expression levels of enhancers are not necessarily proportional to those of epigenomic marks and, for eRNAs whose expression levels are lower (for example, the enhancer that regulates *FTH1* in Fig. 5d), assays that are more effective in capturing unstable transcripts are more likely to recover them. Finally, for the enhancer regulating *TMA16*, signals from histone marks are quite minimal but GRO-cap still captured clear signals of eRNA transcription at this locus, enabling the identification of this enhancer (Fig. 5e).

PINTS web server for exploration and analysis of enhancers. To make it easier for biologists to explore the tens of thousands of candidate enhancers in our compendium, and to prioritize these enhancers for further studies, we constructed an online web server (https://pints.yulab.org) where users can query any human genomic region of interest in a given biological sample to obtain a comprehensive list of candidate enhancers detected by any available TSS assays in that sample using any of the eight peak callers (PINTS, dREG, dREG.HD, FivePrime, GROcapTSSHMM, HOMER, Tfit and TSScall). We have also included detailed annotations for each candidate enhancer, including epigenetic features[57], core promoter elements[64], potential transcription factor binding sites[65] and the presence of population variants and ClinVar mutations[66] (Fig. 6).

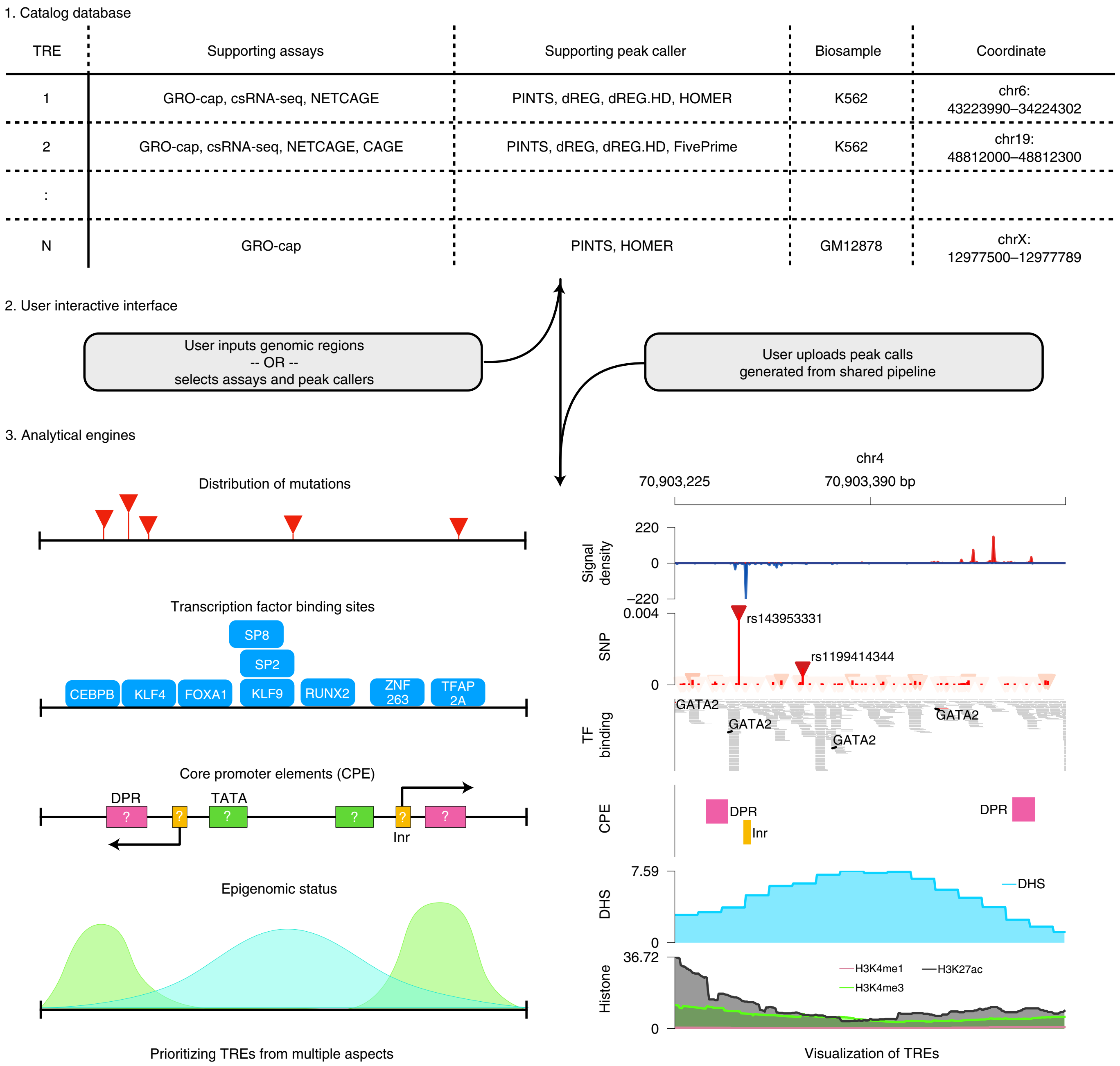

1. Catalog database

TRE	Supporting assays	Supporting peak caller	Biosample	Coordinate
1	GRO-cap, csRNA-seq, NETCAGE	PINTS, dREG, dREG.HD, HOMER	K562	chr6: 43223990–34224302
2	GRO-cap, csRNA-seq, NETCAGE, CAGE	PINTS, dREG, dREG.HD, FivePrime	K562	chr19: 48812000–48812300
:				
N	GRO-cap	PINTS, HOMER	GM12878	chrX: 12977500–12977789

2. User interactive interface

User inputs genomic regions -- OR -- selects assays and peak callers

User uploads peak calls generated from shared pipeline

3. Analytical engines

Fig. 6 | Interactive PINTS web server. The server is composed of three modules: a catalog database containing our human enhancer compendium across 120 biosamples, an interactive user interface and analytical engines. When the user provides genomic loci of their interest as search queries, previously annotated information related to the loci will be retrieved from the catalog database. The user can further refine the search results by a series of filters, including supporting assays, callers, the presence of mutations, transcription factor binding sites, core promoter elements and epigenomic marks. On the other hand, if the user chooses to upload peak calls generated from their data, the analytical engines will analyze the uploads to provide the same types of annotation as those in the catalog database. CPE, core promoter elements; SNP, single nucleotide polymorphism.

Users can prioritize enhancers by requiring the joint presence of specific annotations. For transcription factor binding site analysis, our web server will automatically integrate the information from available RNA-seq data to include only factors expressed in the selected sample.

Furthermore, users can upload their own enhancer calls in a human cell line or tissue; our web server will automatically annotate all of their enhancer calls with the same pipeline as described above. We have integrated epigenomic features and RNA-seq data for 197 human-derived biosamples from the ENCODE project in our web server. For user-uploaded enhancer data in these samples, we automatically refine our annotations by reporting only binding sites of expressed transcription factors and associating each enhancer with epigenomic features specific to the corresponding sample.

Users can explore all annotations of their selected enhancers via our integrated genome browser; alternatively, they can readily export all annotations in plain text format for downstream analyses.

Discussion

Enhancer RNAs are increasingly recognized as a critical marker for active enhancers genome wide[5,6]; however, the optimal strategy (both experimental assays and their analytical pipelines) for detection of eRNAs and thus identification of enhancer loci has not been critically evaluated. In this study we systematically compared 13 in vivo genome-wide RNA-seq assays in K562 cells and showed that TSS assays are in general more sensitive than NT assays in the detection of eRNAs, because signals will not be diluted by active transcription in gene bodies. One additional and critical advantage of TSS assays is that they reveal the precise location of eRNA TSSs, allowing for high-resolution detection and delimitation of enhancer loci genome wide, as demonstrated in our recent work[6]. Overall, our results show that GRO/PRO-cap has the best overall performance in detection of active enhancers in terms of both sensitivity and specificity. Thus, for fresh cells and tissue specimens, or in samples with high RNA quality, we recommend GRO/PRO-cap based on our observations in this study. Because run-on cap assays require an enzymatically active RNA polymerase and cap structure, other TSS assays (for example, FFPEcap-seq[67]) or certain NT assays[18] may perform better on samples where these requirements cannot be met (for example, for paraffin-embedded, formalin-fixed samples).

We noticed that, when using current computational tools to identify TREs from various RNA sequencing datasets, minor changes in sample processing could lead to changes of up to >20% in the final results, which brings the robustness of the peak calls into question. To address this issue we introduced a computational tool, PINTS. Our benchmarks indicate that PINTS achieves the optimal balance among robustness, applicability, sensitivity and specificity, especially for TSS assays capable of detecting the precise location of eRNA TSSs.

In this study we used CRISPR–Cas9- and CRISPRi-validated enhancers[29–37] as the positive reference set, and MPRA/STARR-seq negative segments[6,38–44] as non-enhancers. Although these two sets show quite different epigenomic profiles (Extended Data Fig. 4a), which indicates that our non-enhancer set is depleted of true enhancers, there may still be a few false negatives in the non-enhancer set. This is because, in published MPRA/STARR-seq datasets, only a very small number of promoters was used to test all candidate elements but some enhancers might not work with these promoters. Furthermore, some tested elements might be truncated due to either synthesis limitations (<200 bp) or random fragmentation of the genome. However, such cases are not expected to affect our relative ranking of different assays and thus will have minimal impact on our conclusions. We also note that the features defining enhancers and non-enhancers, both at structural and functional levels, are still a work in progress and, while it appears that the vast majority of active enhancers are transcribed, an accurate estimation of the fraction of enhancers that can initiate transcription remains unknown.

Furthermore, we provide a detailed, comprehensive human enhancer compendium with a unified definition[6,7] of enhancers based on the detected divergent pairs of eRNA TSSs. Such a robust, unified and comprehensive catalog of enhancers across 120 cell types and tissues is expected to shine a light on the mechanism of gene regulation and architectural details of enhancers in general. The precise definition of enhancer element boundaries afforded by TSS assays like PRO/GRO-cap would alleviate potential concerns regarding whether full-length enhancer elements are selected and tested in follow-up functional studies, and thus improve coverage of elements by elimination of incomplete or ill-defined candidates. Such a well-defined catalog of enhancers also provides an invaluable resource for follow-up studies to better understand the similarities and key differences in gene regulation across various tissues and conditions, and to identify key enhancers whose malfunctions can lead to specific disorders.

Online content

Any methods, additional references, Nature Research reporting summaries, source data, extended data, supplementary information, acknowledgements, peer review information; details of author contributions and competing interests; and statements of data and code availability are available at https://doi.org/10.1038/s41587-022-01211-7.

Received: 3 June 2021; Accepted: 6 January 2022;
Published online: 17 February 2022

References

1. Heintzman, N. D. et al. Distinct and predictive chromatin signatures of transcriptional promoters and enhancers in the human genome. *Nat. Genet.* **39**, 311–318 (2007).
2. Calo, E. & Wysocka, J. Modification of enhancer chromatin: what, how, and why? *Mol. Cell* **49**, 825–837 (2013).
3. Kim, T.-K. et al. Widespread transcription at neuronal activity-regulated enhancers. *Nature* **465**, 182–187 (2010).
4. Descostes, N. et al. Tyrosine phosphorylation of RNA polymerase II CTD is associated with antisense promoter transcription and active enhancers in mammalian cells. *eLife* **3**, e02105 (2014).
5. Andersson, R. et al. An atlas of active enhancers across human cell types and tissues. *Nature* **507**, 455–461 (2014).
6. Tippens, N. D. et al. Transcription imparts architecture, function and logic to enhancer units. *Nat. Genet.* **52**, 1067–1075 (2020).
7. Core, L. J. et al. Analysis of nascent RNA identifies a unified architecture of initiation regions at mammalian promoters and enhancers. *Nat. Genet.* **46**, 1311–1320 (2014).
8. Tome, J. M., Tippens, N. D. & Lis, J. T. Single-molecule nascent RNA sequencing identifies regulatory domain architecture at promoters and enhancers. *Nat. Genet.* **50**, 1533–1541 (2018).
9. Kruesi, W. S., Core, L. J., Waters, C. T., Lis, J. T. & Meyer, B. J. Condensin controls recruitment of RNA polymerase II to achieve nematode X-chromosome dosage compensation. *eLife* **2**, e00808 (2013).
10. Kwak, H., Fuda, N. J., Core, L. J. & Lis, J. T. Precise maps of RNA polymerase reveal how promoters direct initiation and pausing. *Science* **339**, 950–953 (2013).
11. Henriques, T. et al. Widespread transcriptional pausing and elongation control at enhancers. *Genes Dev.* **32**, 26–41 (2018).
12. Kodzius, R. et al. CAGE: cap analysis of gene expression. *Nat. Methods* **3**, 211–222 (2006).
13. Batut, P., Dobin, A., Plessy, C., Carninci, P. & Gingeras, T. R. High-fidelity promoter profiling reveals widespread alternative promoter usage and transposon-driven developmental gene expression. *Genome Res.* **23**, 169–180 (2013).
14. Hirabayashi, S. et al. NET-CAGE characterizes the dynamics and topology of human transcribed cis-regulatory elements. *Nat. Genet.* **51**, 1369–1379 (2019).
15. Duttke, S. H., Chang, M. W., Heinz, S. & Benner, C. Identification and dynamic quantification of regulatory elements using total RNA. *Genome Res.* **29**, 1836–1846 (2019).
16. Policastro, R. A., Raborn, R. T., Brendel, V. P. & Zentner, G. E. Simple and efficient profiling of transcription initiation and transcript levels with STRIPE-seq. *Genome Res.* **30**, 910–923 (2020).
17. Core, L. J., Waterfall, J. J. & Lis, J. T. Nascent RNA sequencing reveals widespread pausing and divergent initiation at human promoters. *Science* **322**, 1845–1848 (2008).
18. Nojima, T. et al. Mammalian NET-seq reveals genome-wide nascent transcription coupled to RNA processing. *Cell* **161**, 526–540 (2015).
19. Paulsen, M. T. et al. Coordinated regulation of synthesis and stability of RNA during the acute TNF-induced proinflammatory response. *Proc. Natl Acad. Sci. USA* **110**, 2240–2245 (2013).
20. Magnuson, B. et al. Identifying transcription start sites and active enhancer elements using BruUV-seq. *Sci. Rep.* **5**, 17978 (2015).
21. Chen, H. et al. A pan-cancer analysis of enhancer expression in nearly 9000 patient samples. *Cell* **173**, 386–399 (2018).
22. Zhang, Z. et al. Transcriptional landscape and clinical utility of enhancer RNAs for eRNA-targeted therapy in cancer. *Nat. Commun.* **10**, 4562 (2019).
23. Azofeifa, J. G. & Dowell, R. D. A generative model for the behavior of RNA polymerase. *Bioinformatics* **33**, 227–234 (2017).
24. Danko, C. G. et al. Identification of active transcriptional regulatory elements from GRO-seq data. *Nat. Methods* **12**, 433–438 (2015).
25. Wang, Z., Chu, T., Choate, L. A. & Danko, C. G. Identification of regulatory elements from nascent transcription using dREG. *Genome Res.* **29**, 293–303 (2019).
26. Chu, T. et al. Chromatin run-on and sequencing maps the transcriptional regulatory landscape of glioblastoma multiforme. *Nat. Genet.* **50**, 1553–1564 (2018).
27. Adiconis, X. et al. Comprehensive comparative analysis of 5′-end RNA-sequencing methods. *Nat. Methods* **15**, 505–511 (2018).
28. Frith, M. C. et al. A code for transcription initiation in mammalian genomes. *Genome Res.* **18**, 1–12 (2008).

29. Thakore, P. I. et al. Highly specific epigenome editing by CRISPR-Cas9 repressors for silencing of distal regulatory elements. *Nat. Methods* **12**, 1143–1149 (2015).
30. Fulco, C. P. et al. Systematic mapping of functional enhancer-promoter connections with CRISPR interference. *Science* **354**, 769–773 (2016).
31. Wakabayashi, A. et al. Insight into GATA1 transcriptional activity through interrogation of cis elements disrupted in human erythroid disorders. *Proc. Natl Acad. Sci. USA* **113**, 4434–4439 (2016).
32. Klann, T. S. et al. CRISPR-Cas9 epigenome editing enables high-throughput screening for functional regulatory elements in the human genome. *Nat. Biotechnol.* **35**, 561–568 (2017).
33. Xie, S., Duan, J., Li, B., Zhou, P. & Hon, G. C. Multiplexed engineering and analysis of combinatorial enhancer activity in single cells. *Mol. Cell* **66**, 285–299 (2017).
34. Gasperini, M. et al. A genome-wide framework for mapping gene regulation via cellular genetic screens. *Cell* **176**, 377–390 (2019).
35. Fulco, C. P. et al. Activity-by-contact model of enhancer-promoter regulation from thousands of CRISPR perturbations. *Nat. Genet.* **51**, 1664–1669 (2019).
36. Xie, S., Armendariz, D., Zhou, P., Duan, J. & Hon, G. C. Global analysis of enhancer targets reveals convergent enhancer-driven regulatory modules. *Cell Rep.* **29**, 2570–2578 (2019).
37. Schraivogel, D. et al. Targeted Perturb-seq enables genome-scale genetic screens in single cells. *Nat. Methods* **17**, 629–635 (2020).
38. Kheradpour, P. et al. Systematic dissection of regulatory motifs in 2000 predicted human enhancers using a massively parallel reporter assay. *Genome Res.* **23**, 800–811 (2013).
39. Kwasnieski, J. C., Fiore, C., Chaudhari, H. G. & Cohen, B. A. High-throughput functional testing of ENCODE segmentation predictions. *Genome Res.* **24**, 1595–1602 (2014).
40. Ulirsch, J. C. et al. Systematic functional dissection of common genetic variation affecting red blood cell traits. *Cell* **165**, 1530–1545 (2016).
41. Ernst, J. et al. Genome-scale high-resolution mapping of activating and repressive nucleotides in regulatory regions. *Nat. Biotechnol.* **34**, 1180–1190 (2016).
42. Maricque, B. B., Chaudhari, H. G. & Cohen, B. A. A massively parallel reporter assay dissects the influence of chromatin structure on cis-regulatory activity. *Nat. Biotechnol.* **37**, 90–95 (2019).
43. Rathert, P. et al. Transcriptional plasticity promotes primary and acquired resistance to BET inhibition. *Nature* **525**, 543–547 (2015).
44. Dao, L. T. M. et al. Genome-wide characterization of mammalian promoters with distal enhancer functions. *Nat. Genet.* **49**, 1073–1081 (2017).
45. Lee, D. et al. STARRPeaker: uniform processing and accurate identification of STARR-seq active regions. *Genome Biol.* **21**, 298 (2020).
46. Wang, X. et al. High-resolution genome-wide functional dissection of transcriptional regulatory regions and nucleotides in human. *Nat. Commun.* **9**, 5380 (2018).
47. Schwalb, B. et al. TT-seq maps the human transient transcriptome. *Science* **352**, 1225–1228 (2016).
48. Core, L. J. et al. Defining the status of RNA polymerase at promoters. *Cell Rep.* **2**, 1025–1035 (2012).
49. Mchaourab, Z. F., Perreault, A. A. & Venters, B. J. ChIP-seq and ChIP-exo profiling of Pol II, H2A.Z, and H3K4me3 in human K562 cells. *Sci. Data* **5**, 180030 (2018).
50. Harrow, J. et al. GENCODE: the reference human genome annotation for The ENCODE Project. *Genome Res.* **22**, 1760–1774 (2012).
51. O'Leary, N. A. et al. Reference sequence (RefSeq) database at NCBI: current status, taxonomic expansion, and functional annotation. *Nucleic Acids Res.* **44**, D733–D745 (2016).
52. Jurka, J. Repbase update: a database and an electronic journal of repetitive elements. *Trends Genet.* **16**, 418–420 (2000).
53. Djebali, S. et al. Landscape of transcription in human cells. *Nature* **489**, 101–108 (2012).
54. Field, A. & Adelman, K. Evaluating enhancer function and transcription. *Annu. Rev. Biochem.* **89**, 213–234 (2020).
55. Andersson, R. & Sandelin, A. Determinants of enhancer and promoter activities of regulatory elements. *Nat. Rev. Genet.* **21**, 71–87 (2020).
56. Palazzo, A. F. & Koonin, E. V. Functional long non-coding RNAs evolve from junk transcripts. *Cell* **183**, 1151–1161 (2020).
57. ENCODE Project Consortium et al. Expanded encyclopaedias of DNA elements in the human and mouse genomes. *Nature* **583**, 699–710 (2020).
58. Wang, D. et al. Reprogramming transcription by distinct classes of enhancers functionally defined by eRNA. *Nature* **474**, 390–394 (2011).
59. Chae, M., Danko, C. G. & Kraus, W. L. groHMM: a computational tool for identifying unannotated and cell type-specific transcription units from global run-on sequencing data. *BMC Bioinformatics* **16**, 222 (2015).
60. Zhang, Y. et al. Model-based analysis of ChIP-Seq (MACS). *Genome Biol.* **9**, R137 (2008).
61. Schneider, V. A. et al. Evaluation of GRCh38 and de novo haploid genome assemblies demonstrates the enduring quality of the reference assembly. *Genome Res.* **27**, 849–864 (2017).
62. Roadmap Epigenomics Consortium et al. Integrative analysis of 111 reference human epigenomes. *Nature* **518**, 317–330 (2015).
63. Pennacchio, L. A., Bickmore, W., Dean, A., Nobrega, M. A. & Bejerano, G. Enhancers: five essential questions. *Nat. Rev. Genet.* **14**, 288–295 (2013).
64. Vo Ngoc, L., Huang, C. Y., Cassidy, C. J., Medrano, C. & Kadonaga, J. T. Identification of the human DPR core promoter element using machine learning. *Nature* **585**, 459–463 (2020).
65. Fornes, O. et al. JASPAR 2020: update of the open-access database of transcription factor binding profiles. *Nucleic Acids Res.* **48**, D87–D92 (2020).
66. Landrum, M. J. et al. ClinVar: improvements to accessing data. *Nucleic Acids Res.* **48**, D835–D844 (2020).
67. Vahrenkamp, J. M. et al. FFPEcap-seq: a method for sequencing capped RNAs in formalin-fixed paraffin-embedded samples. *Genome Res.* **29**, 1826–1835 (2019).

Publisher's note Springer Nature remains neutral with regard to jurisdictional claims in published maps and institutional affiliations.

Methods

Data preprocessing. All datasets were managed and analyzed with BioQueue[68] (accession numbers for these datasets are available in Supplementary Table 1). Raw reads were preprocessed with fastp[69] for adapter trimming. Only reads >14 bp were kept for downstream analyses. All processed reads from RNA assays were aligned using STAR[70] to primary assemblies of human reference genome hg38 (GCF_000001305.15) together with ribosomal DNA (U13369.1), with the parameters as–outSAMattributes All–outSAMmultNmax 1–outFilterMultimapNmax 50. For studies using *Drosophila* cells, or other specific samples as spike-ins, either the *Drosophila* reference genome (dm6) or the corresponding reference sequences used in the original studies were incorporated into the index (details available in Supplementary Table 1). To measure the robustness of peak prediction, we also mapped reads to primary assemblies of human reference genome hg19 (from the University of California, Santa Cruz (UCSC); sequences from alternative loci/haplotypes were removed in the same way as for hg38). Reads from DNA assays were aligned and processed using bwa[71] and samtools[72] with default parameters.

Determination of read coverage among reference regions. Sequencing reads of replicates for the same assay were merged and downsampled to the same sequencing depth (the same number of mappable reads) three times using picard with the parameter STRATEGY = Chained. These downsampled data were then converted to bed files to calculate the fraction of overlap between sequencing reads and reference regions in a strand-specific manner.

Classification of transcription units as stable and unstable units with TT-seq. Transcript annotations derived from transient transcriptome sequencing (TT-seq; GSE75792 (ref. [47])) were downloaded from the GEO database. Transcription units with any missing values were discarded. The 95th quantile of estimated decay rates for mRNAs was used as the cutoff between unstable (above the cutoff) and stable (below the cutoff) transcription units.

Characterization of the genome-wide distribution of reads. The entire genome was classified into four categories based on the annotations in GENCODE v.24 (ref. [50]): exonic and intronic regions were defined as in GENCODE, except that any region with overlapping intronic and exonic annotation was considered as exonic; the 500-bp regions flanking annotated transcription start sites of protein-coding transcripts were annotated as promoters, while all other regions were considered as intergenic. Sequencing reads of various assays were assigned to the categories of promoters, introns, exons or intergenic regions (in the exact order) if they were aligned to the corresponding annotated regions in the genome.

Identification of sequencing reads from splicing intermediates. The exact or approximate positions of transcript termini were inferred from the read ends, and the abundance of their corresponding transcripts was normalized as reads per million (RPM) for this analysis. A list of annotated splice junctions and their 200-bp flanking regions in the human genome was compiled based on GENCODE v.24 (ref. [50]). For each assay, we iterated through this list and recorded normalized read counts at each position. In Extended Data Fig. 3e, both the average of signals and the 95% CI (estimated by bootstrap) of averages are reported.

Compiling the reference sets. The experimentally quantified enhancer activity of various DNA elements was collected from previous studies (enhancers: 938 from CRISPR[31] or CRISPRi[29,30,32–37]; non-enhancers: 20,941 from STARR-seq[6,43,44] and 17,462 from MPRA[38–42]). Overlapping elements within the same category were merged until the resulting elements overlapped with elements in the other category. Non-enhancer loci were excluded in the final set if (1) they were <250 bp; (2) they overlapped with PLS or ELS predicted by cCRE[57]; or (3) they overlapped with potential promoters (1-kb regions flanking TSSs in GENCODE). When selecting MPRA-[38–42] and STARR-seq-[6,43–45] identified enhancers in K562, we required supporting data from at least two independent studies to ameliorate the inclusion of false-positive enhancers resulting from orientation bias (STARR-seq) or promoter activity (MPRA). For GM12878, to ameliorate false positives caused by orientation bias only orientation-independent enhancer calls from HiDRA were used[6,46].

Calculation of FDR for assays. multiBamSummary[73] was used to generate tables of read counts across the genome in 500-bp bins. For each assay, bins were ranked by counts in them, with the top *n* bins considered as true signals from the assay (four cutoffs were tested: 5,000, 10,000, 20,000 and 100,000; Extended Data Fig. 4d). If a bin overlapped with a locus in the CRISPR-identified enhancer set, that bin was considered a true positive (TP); if a bin overlapped with a locus in the non-enhancer set, it was considered a false positive (FP). FDR was calculated as:

$$\mathrm{FDR} = \frac{\sum \mathrm{FP}}{\sum \mathrm{TP} + \sum \mathrm{FP}}$$

PINTS. Briefly, read ends were separated based on their mapping directions on the reference genome (forward or reverse), and read counts were binned into 100-bp windows. Adjacent windows with reads available were merged to avoid splitting of potential TRE elements. Within each window, the algorithm first finds peak seeds using a prominence-based approach. Then with a maximum-scoring pairing strategy[28], nearby seeds will be merged as peak candidates if density (D) after merging meets the following condition:

$$D_{\mathrm{merged}} \geq \alpha \times \min(\{D_{\mathrm{seed1}}, D_{\mathrm{seed2}}\})$$

The default value for α is 1, and PINTS resolution can be further fine-tuned by incorporating reference annotations. For example, when the transcript annotation is available, PINTS will try to avoid overlap of peak candidates with more than one transcript.

Next, to address the increased sparsity of signals when only the read ends are taken into account, the expectation-maximization algorithm is used to fit zero-inflated Poisson (ZIP) models to both peak candidates and their neighborhood regions (λ for read density, π for the proportion of zeros not derived from a Poisson process), and the probability mass function of these models has the following form:

$$\Pr\left(X = x\right) = \begin{cases} \pi + (1-\pi)\, e^{-\lambda}, x = 0 \\ (1-\pi) e^{-\lambda} \frac{\lambda^x}{x!}, x > 0 \end{cases}$$

Assuming an unobservable latent random variable z_i for a window X of I observations the complete log-likelihood is proportional to

$$\ln L \propto \sum_{i=1}^{I} \left[z_i \ln\left(\pi\right) + (1-z_i) \ln\left(1-\pi\right) + (1-z_i)\left(-\lambda + x_i \ln \lambda\right)\right]$$

In E-step at the $(r+1)$th iteration, z_i is estimated by its conditional expectation:

$$\hat{z}_i^{(r+1)} = \begin{cases} \frac{\hat{\pi}^{(r)}}{\hat{\pi}^{(r)} + e^{-\hat{\lambda}^{(r)}}\left(1-\hat{\pi}^{(r)}\right)}, & x_i = 0 \\ 0, & x_i > 0 \end{cases}$$

In M-step, given $\hat{z}_i^{(r+1)}$, the estimations of π and λ are updated as follows:

$$\hat{\pi}^{(r+1)} = \frac{\sum_{i=1}^{I} \hat{z}_i^{(r+1)}}{I}$$

$$\hat{\lambda}^{(r+1)} = \frac{\sum_{i=1}^{I}\left(1-\hat{z}_i^{(r+1)}\right) x_i}{\sum_{i=1}^{I}\left(1-\hat{z}_i^{(r+1)}\right)}$$

An IQR-based refinement is applied before fitting ZIP models to neighborhood regions. In this case, if certain peak candidates in a local environment are considered as outliers by IQR (their densities are >Q3 + 1.5 × IQR, where IQR = Q3 – Q1), these candidates will be masked. For libraries with low sequencing depth, rather than simultaneously masking all outlier peak candidates in the local background, PINTS masks one peak candidate at a time and calculates the resulting peak density in the local background. The process is reiterated until PINTS either identifies the outlier candidates or reports the nonexistence of such outliers. The estimated densities are then used to determine statistically significant peaks, which are further categorized into divergent peak pairs (peaks on opposite strands and within 300 bp) and unidirectional peaks.

For enhancer-like elements that do not pass the statistical cutoff of PINTS but have clear enhancer-related epigenomic marks, PINTS will offer an option to include these elements in the output where they will be labeled as 'marginal', and their corresponding epigenomic marks. To use this feature, the user needs to add –epig-annotation <biosample> when running PINTS.

PINTS depends on open-source Python packages including numpy[74], scipy[75], pandas, statsmodels[76], pybedtools[77], pyBigWig, pysam and biopython[78].

Generation of peak calls with existing tools. Peak calls for different assays were made using default parameters for other existing peak callers, with the following exceptions. For MACS2, –keep-dup all was set so that reads mapped to the same loci would be retained. For FivePrime, parameters $D_{\min}$, $P_{\min}$ and $S_{\min}$ were optimized according to the sequencing depth of corresponding libraries, and both divergent TSS calls and enhancer calls were combined as the final output. All tools were allowed to create up to 16 threads/subprocesses if they allowed multithreading or parallel computing. For peak callers that do not primarily identify divergent peaks, unidirectional peaks were paired providing they were within 300 bp and on opposite strands. Maximum memory usage and CPU time (sum of all threads) were monitored with help from BioQueue[68]. UCSC Genome Browser command line tools (bedToBigBed, bigBedToBed, bigWigToBedGraph, bedGraphToBigWig and bigWigMerge) and bedtools[79] were used for the conversion of file formats. All peak calls were generated on machines with Intel Xeon Gold 6152 CPU at 2.10 GHz with 88 cores and 1,006 GB of random-access memory running CentOS 7.6.1810.

Evaluation of the systematic biases of different peak-calling methods. For each assay, divergent elements were identified using all applicable peak callers, including PINTS. To accommodate the size difference in these elements as well as elements in the CRISPR-identified enhancer set, a 1,000-bp region centered around the midpoint of each element was used to evaluate the performance of different methods.

Evaluation of the upper bound of peak caller robustness. Sequencing reads were aligned to another popular reference genome sequence, hg19, and divergent elements were identified accordingly with different peak callers. Peak calls generated from both genome releases were cross-lifted using UCSC's liftover, and the average between the two Jaccard indices was considered as the upper bound robustness (UBR):

$$\mathrm{UBR} = \frac{1}{2} \times \left(\frac{|\mathrm{Peaks}_{38} \cap \mathrm{Peaks}_{19\rightarrow 38}|}{|\mathrm{Peaks}_{38} \cup \mathrm{Peaks}_{19\rightarrow 38}|} + \frac{|\mathrm{Peaks}_{19} \cap \mathrm{Peaks}_{38\rightarrow 19}|}{|\mathrm{Peaks}_{19} \cup \mathrm{Peaks}_{38\rightarrow 19}|} \right)$$

ROCs. For each assay, any element from the CRISPR-identified and non-enhancer sets was filtered out if there were no sequencing reads aligned to both strands of the element. The positive set was composed of an equal number of randomly sampled promoters (1-kb regions flanking TSSs in GENCODE v.24) from expressed genes and filtered enhancers. The negative set was composed of the filtered non-enhancers. Receiver operating characteristics (ROCs) were generated by calculating the number of divergent elements overlapping with the positive and negative sets under different cutoffs of scores: *P* values of peaks for PINTS and MACS2, FDRs for TSScall, output support vector regression (SVR) scores for dREG, likelihood ratio scores for Tfit and peak scores for HOMER (findcsRNATSS.pl and findPeak -style TSS). For dREG.HD, GROcapTSSHMM, FivePrime and HOMER (GRO-seq), since there are either no scores or multiple scores returned in the final output, sensitivity and specificity were evaluated and reported with their default parameters.

PINTS web server. The PINTS web server is powered by the Django web framework. dbSNP v.153 (ref. [80]) was used for annotation of mutations among TREs; JASPAR 2020 (ref. [65]) was employed for annotation of transcription factor registries, and only TFs expressed in the corresponding biosample (based on RNA-seq data from ENCODE) were included (see Supplementary Table 4 for a list of datasets used and accession information). cCRE v.254 (ref. [57]) was used for epigenomic annotation. Core promoter elements were annotated using the following strategy: for each major TSS (+1), the portal annotated the elements as having either an initiator or an initiator-like element when the sequence of -3~+3 matches BBCABW, or the sequence of +1~+2 matches YR, respectively. The TATA box (−32~−21) and DPR elements (+17~+35) were identified using the previously published SVR model[64].

Reporting Summary. Further information on research design is available in the Nature Research Reporting Summary linked to this article.

Data availability

Processed TRE calls are publicly accessible via our web portal (https://pints.yulab.org). Data that support the findings of this study are available within the paper and its Supplementary information files. All sequencing data analyzed in this study were retrieved from public databases (NCBI GEO and ENCODE portal); lists of accessions are available in Supplementary Tables 1 and 4. Source data are provided with this paper.

Code availability

The source code of PINTS is publicly available at https://github.com/hyulab/PINTS; scripts and pipelines used to generate results reported in this study can be retrieved from https://github.com/hyulab/PINTS_analysis.

References

68. Yao, L., Wang, H., Song, Y. & Sui, G. BioQueue: a novel pipeline framework to accelerate bioinformatics analysis. *Bioinformatics* **33**, 3286–3288 (2017).
69. Chen, S., Zhou, Y., Chen, Y. & Gu, J. fastp: An ultra-fast all-in-one FASTQ preprocessor. *Bioinformatics* **34**, i884–i890 (2018).
70. Dobin, A. et al. STAR: ultrafast universal RNA-seq aligner. *Bioinformatics* **29**, 15–21 (2013).
71. Li, H. & Durbin, R. Fast and accurate short read alignment with Burrows–Wheeler transform. *Bioinformatics* **25**, 1754–1760 (2009).
72. Li, H. et al. The Sequence Alignment/Map format and SAMtools. *Bioinformatics* **25**, 2078–2079 (2009).
73. Ramírez, F. et al. deepTools2: a next generation web server for deep-sequencing data analysis. *Nucleic Acids Res.* **44**, W160–W165 (2016).
74. Harris, C. R. et al. Array programming with NumPy. *Nature* **585**, 357–362 (2020).
75. Virtanen, P. et al. SciPy 1.0: fundamental algorithms for scientific computing in Python. *Nat. Methods* **17**, 261–272 (2020).
76. Seabold, S. & Perktold, J. Statsmodels: econometric and statistical modeling with Python. https://doi.org/10.25080/majora-92bf1922-011 (2010).
77. Dale, R. K., Pedersen, B. S. & Quinlan, A. R. Pybedtools: a flexible Python library for manipulating genomic datasets and annotations. *Bioinformatics* **27**, 3423–3424 (2011).
78. Cock, P. J. A. et al. Biopython: freely available Python tools for computational molecular biology and bioinformatics. *Bioinformatics* **25**, 1422–1423 (2009).
79. Quinlan, A. R. & Hall, I. M. BEDTools: a flexible suite of utilities for comparing genomic features. *Bioinformatics* **26**, 841–842 (2010).
80. Sherry, S. T. et al. dbSNP: the NCBI database of genetic variation. *Nucleic Acids Res.* **29**, 308–311 (2001).
81. Preker, P. et al. RNA exosome depletion reveals transcription upstream of active human promoters. *Science* **322**, 1851–1854 (2008).
82. van Arensbergen, J. et al. Genome-wide mapping of autonomous promoter activity in human cells. *Nat. Biotechnol.* **35**, 145–153 (2017).
83. Shivram, H. & Iyer, V. R. Identification and removal of sequencing artifacts produced by mispriming during reverse transcription in multiple RNA-seq technologies. *RNA* **24**, 1266–1274 (2018).
84. Bedi, K., Paulsen, M. T., Wilson, T. E. & Ljungman, M. Characterization of novel primary miRNA transcription units in human cells using Bru-seq nascent RNA sequencing. *NAR Genom. Bioinform.* **2**, lqz014 (2020).
85. Zacher, B. et al. Accurate promoter and enhancer identification in 127 ENCODE and roadmap epigenomics cell types and tissues by GenoSTAN. *PLoS ONE* **12**, e0169249 (2017).

Acknowledgements

Computation was performed on a cluster administered by the Biotechnology Resource Center at Cornell University. We thank members of the Yu and Lis laboratories and the ENCODE Consortium (specifically A. Mortazavi, M. Ljungman and J. E. Moore) for helpful discussions and guidance; and H. Zhu for her suggestions on concept visualization. This work was supported by grants from the National Institutes of Health (no. UM1HG009393 to J.T.L. and H.Y. and nos. R01DK115398, R01DK127778 and R01HD082568 to H.Y.). L.Y. was supported by the Cornell Presidential Life Sciences Fellowship.

Author contributions

Conceptualization was performed by L.Y., J.T.L. and H.Y. Methodology was carried out by L.Y. Software was the responsibility of L.Y. L.Y. carried out formal analysis. J.L. performed investigations. Data curation was carried out by L.Y., J.L. and A.K.-Y.L. L.Y. and J.L. wrote the original draft. Writing, review and editing were performed by J.L., A.O., J.T.L. and H.Y. Visualization was the responsibility of L.Y., J.L., A.O. and H.Y. J.T.L. and H.Y. supervised the study.

Competing interests

The authors declare no competing interests.

Additional information

Extended data is available for this paper at https://doi.org/10.1038/s41587-022-01211-7.

Supplementary information The online version contains supplementary material available at https://doi.org/10.1038/s41587-022-01211-7.

Correspondence and requests for materials should be addressed to John T. Lis or Haiyuan Yu.

Peer review information *Nature Biotechnology* thanks Leng Han and the other, anonymous, reviewer(s) for their contribution to the peer review of this work.

Reprints and permissions information is available at www.nature.com/reprints.

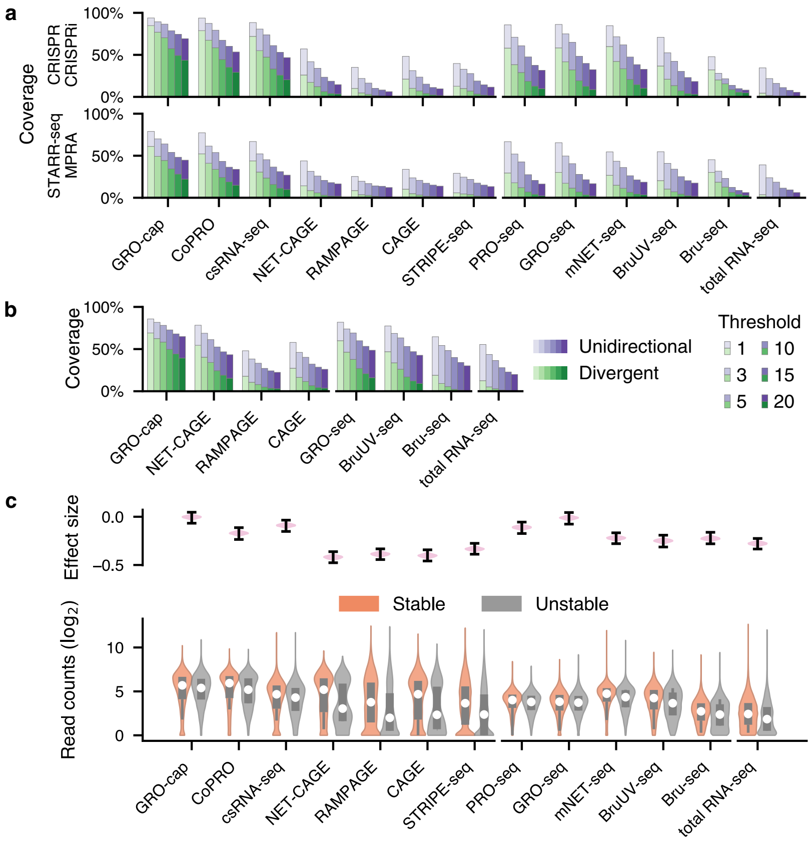

Extended Data Fig. 1 | An extended evaluation of eRNA detection sensitivity of different assays. a and **c** are the extended versions for Fig. 2a,b, respectively. **a** and **b** show the capability of different assays to capture previously identified enhancers. The color of stacked bars indicates the detection of eRNAs originated from either one or both strands of the enhancer loci. The transparency level shows the number of reads for an enhancer locus to be considered as covered. The top track in **a** is derived from the CRISPR or CRISPRi based reference set (*n* = 803), the bottom track is derived from consensus loci validated by STARR-seq and MPRA (*n* = 550). **b**, Sensitivity evaluated in the other cell line, GM12878, with orientation-independent enhancers identified from previous studies (*n* = 3,544)[6,46]. **c**, Differences in read coverage among stable (*n* = 13,861) and unstable (*n* = 6,380) transcripts. The error bars in the top track show the extrema of effect sizes (*n* = 5,000). The center dots, box limits, and whiskers in the bottom track of **c** denote the median, upper and lower quartiles, and 1.5× interquartile range, respectively.

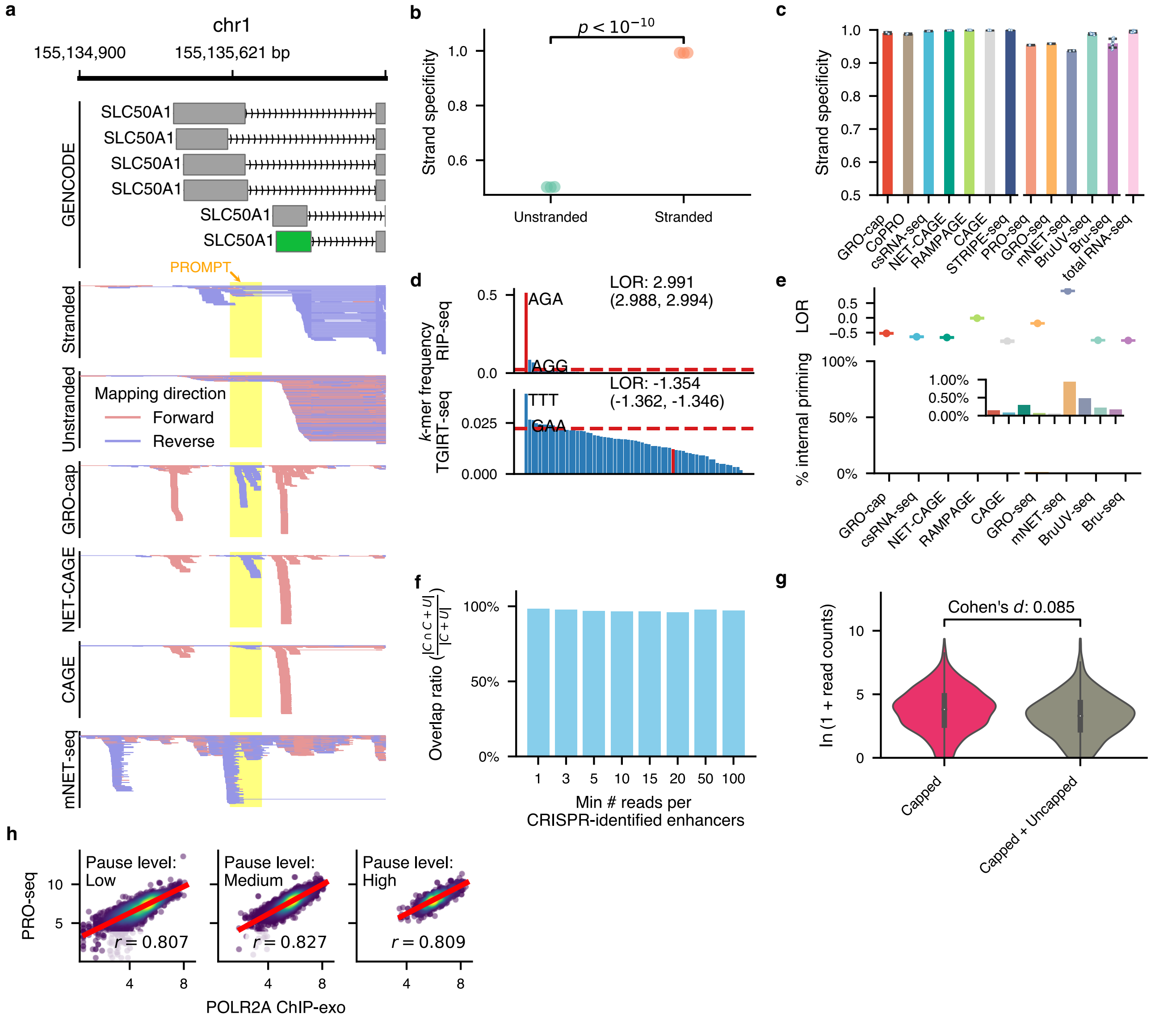

Extended Data Fig. 2 | Effect of technical artifacts on eRNA capture. **a**, A new strategy for evaluating strand specificity without the interference from promoter-upstream transcripts (PROMPTs)[81]. Red and blue colors indicate reads' mapping direction; the highlighted (yellow) region indicates a previously validated[82] PROMPT. Only the first exon in green was used for evaluation. **b**, Strand specificities of three stranded and unstranded RNA-seq libraries with our strategy. The *p*-value was estimated by a two-sided *t* test; **c**, Strand specificity for all libraries evaluated with our strategy. Values and error bars represent the mean and SD. *n* = 2 (GRO-cap, CoPRO, csRNA-seq, PRO-seq, GRO-seq, mNET-seq), *n* = 3 (STRIPE-seq), *n* = 4 (CAGE and RAMPAGE), *n* = 8 (BruUV-seq, total RNA-seq), *n* = 9 (Bru-seq). **d**, Distribution of 3-mers at flush end sites[83] for RIP-seq and TGIRT-seq. The dashed red lines stand for the frequency of RT3-mers (sequence identical to the last three nts for the RT primer [for RIP-seq] or the 3′ adapter [for TGIRT-seq]) in the genome. **e**, Log odds ratios (LORs) of observed RT3-mer at flushing end sites versus in the genome (top) and internal priming rates (bottom) of assays when the internal priming could be detected from the sequencing data. **f**, The overlap between enhancers in the RppH library (Capped+Uncapped as 'C + U') that are also covered in the Capped library (C). The *x*-axis shows the minimum number of reads required for an enhancer locus to be considered as covered. **g**, Difference of log-transformed read counts between the capped (C) and RppH (C + U) libraries. The effect size was measured by Cohen's *d*. In the box plot, the center dots, box limits, and whiskers denote the median, upper and lower quartiles, and 1.5× interquartile range, respectively. **h**, Pearson's *r* of log-transformed reads from promoters of expressed transcripts (TPM > 5) was quantified using PRO-seq and POLR2A ChIP-exo. *n* = 4,747 (low), *n* = 9,058 (medium), and *n* = 2,470 (high).

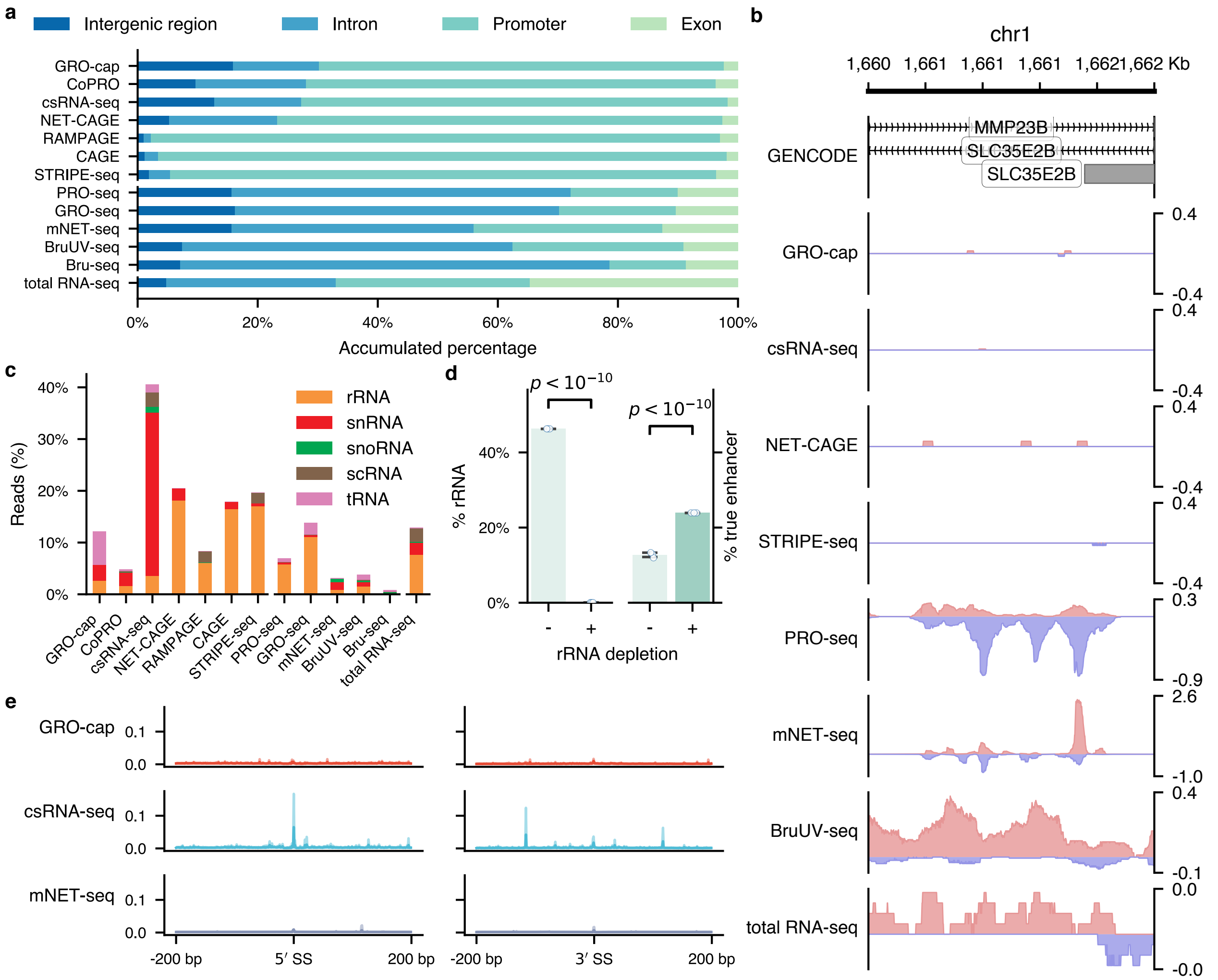

Extended Data Fig. 3 | Analyses of factors affecting assays' sensitivity in detecting eRNAs. a is the extended version for Fig. 3a. **b**, An example shows that divergent transcripts detected by NT-assays can originate from two overlapping genes (*MMP23B* and *SLC35E2B*) instead of from a regulatory element. Sequencing reads were RPM-normalized. **c**, Proportion of mappable reads from different assays originated from various abundant RNA families. **d**, Effects of rRNA depletion in eRNA enrichment. For each category, three downsampled libraries were included. BruUV-seq libraries from a previously published study[84] were used for this analysis. The *p*-value for rRNA percentage was calculated by two proportions *z* test (two-sided, *p*-value: 0); the *p*-value for true enhancer coverage was calculated by McNemar's test (two-sided, *p*-value: 2.1×10^{-25}). Values and error bars represent the mean and SD. **e**, The distribution of sequencing reads (in RPM) around GENCODE-annotated splicing junction sites. The shaded area indicates the 95% confidence interval of mean values estimated via bootstrap.

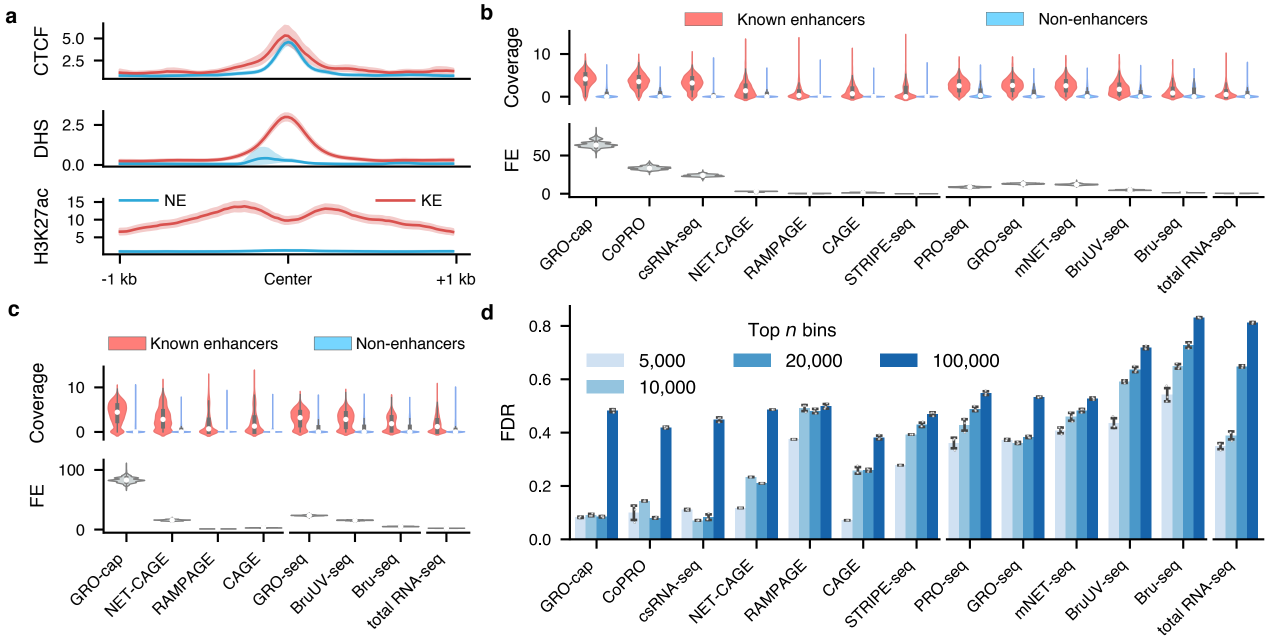

Extended Data Fig. 4 | Extended evaluations of assays' specificity. **a**, Epigenomic and transcription factor binding profiles for the enhancer and non-enhancer sets. For H3K27ac and CTCF, the profiles are presented as fold-changes over control; for DHS, the profile is shown as normalized sequencing depth. Solid lines represent mean densities, and shades depict the 95% confidence interval of mean values estimated via bootstrap. KE: known enhancers; NE: non-enhancers. **b** Signal-to-noise ratios evaluated in K562. *n* = 803 for known enhancers, *n* = 6,777 for non-enhancers. **c**, Signal-to-noise ratios evaluated in GM12878. *n* = 3,544 (Known enhancers), and *n* = 153,809 (Non-enhancers). For **b** and **c**, 10,000 bootstrapped samples were used for calculating the fold enrichment (FE). The center dots, box limits, and whiskers in **b** and **c** denote the median, upper and lower quartiles, and 1.5× interquartile range, respectively. **d**, False discovery rates estimated by the overlap between the top 5,000, 10,000, 20,000, and 100,000 genomic bins and the true and non-enhancer sets. Downsampled libraries were used (*n* = 3); values and error bars represent the mean and SD.

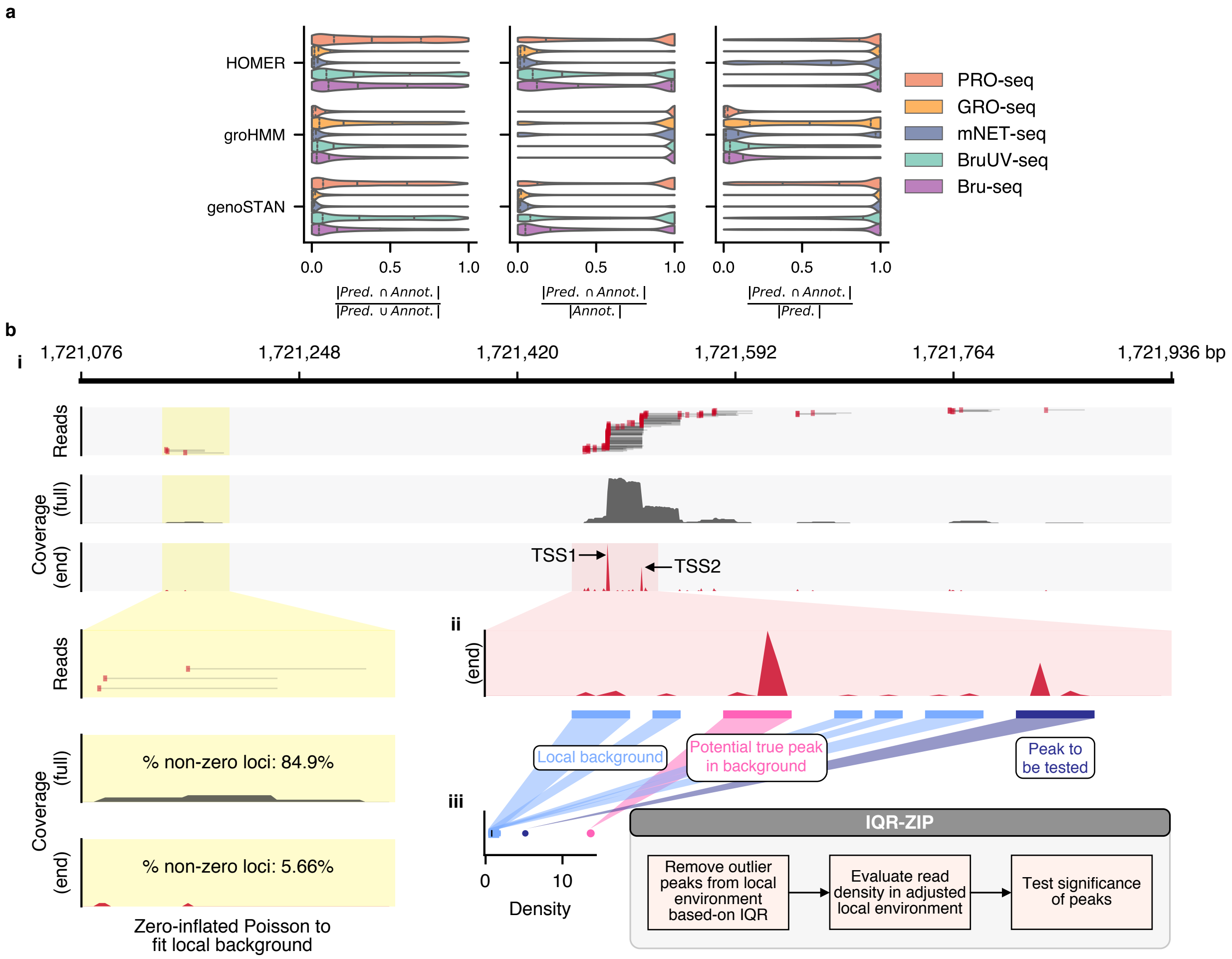

Extended Data Fig. 5 | Assessments of transcript unit prediction and schematic illustration of PINTS. a, The consistencies vary greatly between transcription units annotated in GENCODE (Annot.) and those predicted by different tools[58,59,85] (Pred.). Lines in the violin plot indicate the 25th, 50th, and 75th quartiles, respectively. **b**, Schematic plot of PINTS. **i**, Improvement of TSS identification resolution by focusing only on read ends and using zero-inflated Poisson (ZIP) models to fit local background to address the substantially increased sparsity of signals. The thin grey lines indicate sequencing reads with the 5′ ends highlighted in red. **ii**, The existence of other potential true peaks (pink) elevates the estimation of read density in the local background. **iii**, A schematic plot shows how IQR-ZIP works. The blue box shows the read density distribution of the local background; the purple dot shows the density of the peak to be tested; the pink dot shows the density of a potential true peak close to the peak to be tested, whose read density is a clear outlier and thus excluded from local background estimation.

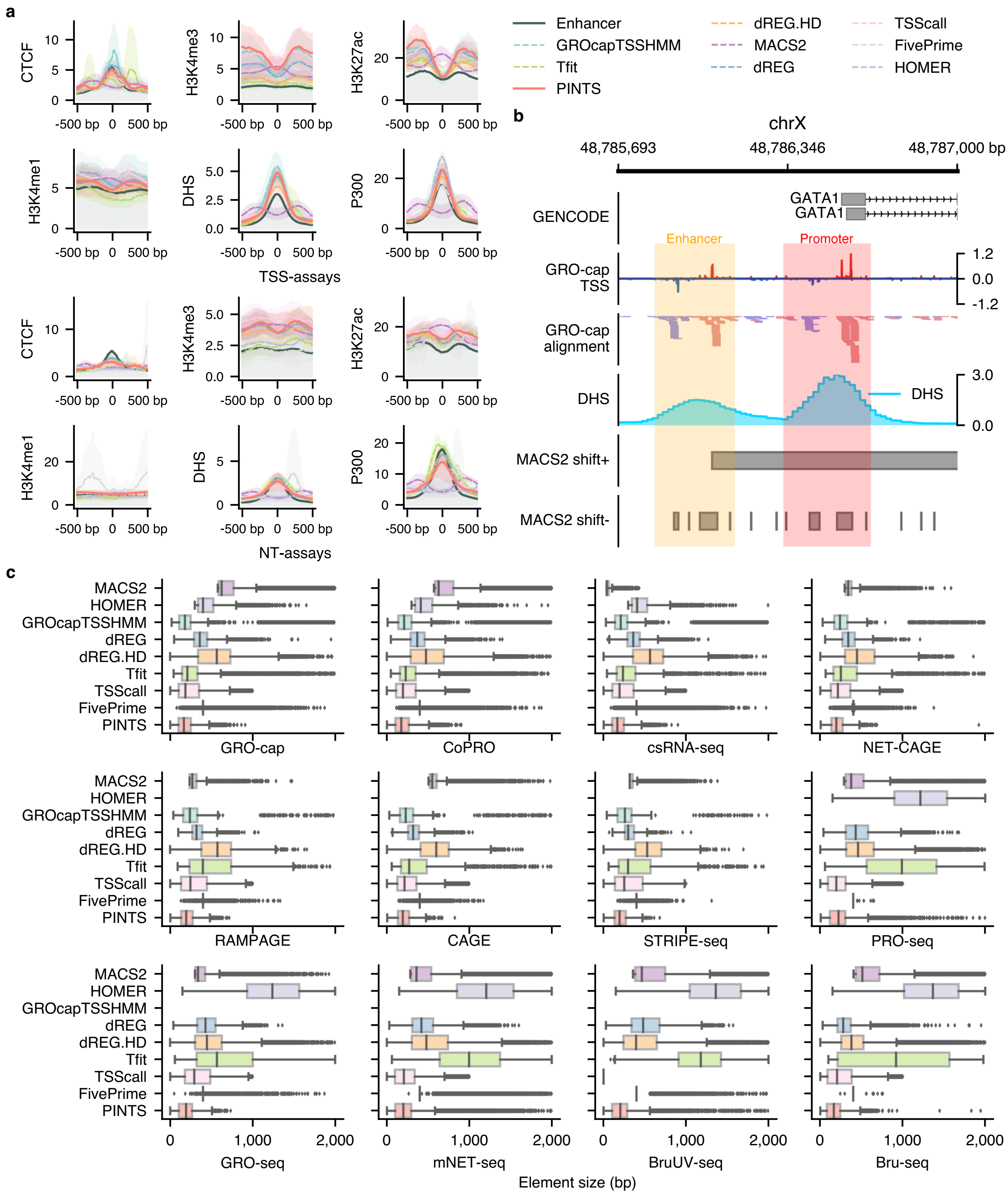

Extended Data Fig. 6 | Profiles of peak calls generated by different peak callers for various assays. a, Aggregated profiles of epigenomic marks, transcription binding sites, and chromatin accessibility in true enhancer regions and distal TREs identified by different peak callers for TSS- and NT-assays. The shaded area indicates the 95% confidence interval of mean values estimated via bootstrap; **b**, An example demonstrating why MACS2 is not suitable for identifying TREs. **c**, Distribution of element sizes identified from 12 assays by all applicable peak callers. In the box plot, the center lines, box limits, and whiskers denote the median, upper and lower quartiles, and 1.5× interquartile range, respectively; points show observations that are not in the range of quartiles ±1.5 × (Q_3 – Q_1). A table of sample sizes is available in Supplementary Table 5.

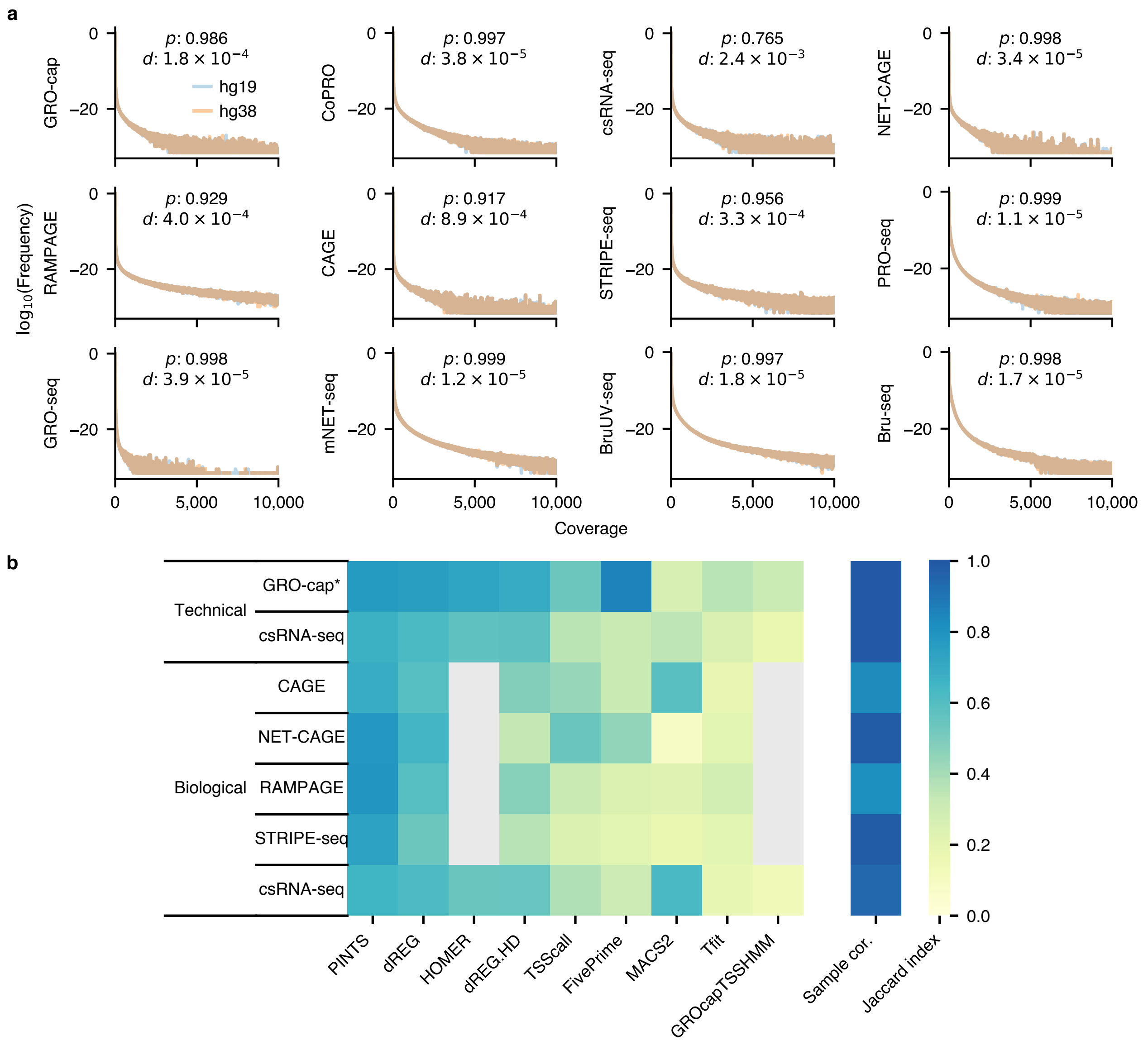

Extended Data Fig. 7 | Extended analyses on the robustness of element predictions. a, A previous study showed that the sequences between hg19 and hg38 are very similar as hg38 has 0.09% more ungapped non-centromeric sequences than hg19, only 0.17% of ungapped hg19 sequences are not in hg38[61]. Here we show the distribution of sequencing reads in the genome. The read counts of each assay were summarized against their frequency in a log scale with hg19 as blue lines and hg38 as orange lines. The *p*-values were calculated by two-sided Student's *t* tests. **b**, Robustness (Jaccard index) of different peak callers when applying them to experimental data with technical and biological replicates. Correlations between alignments (Sample cor.) were calculated as Pearson's *r* of log-transformed read counts among genomic bins (500 bp).

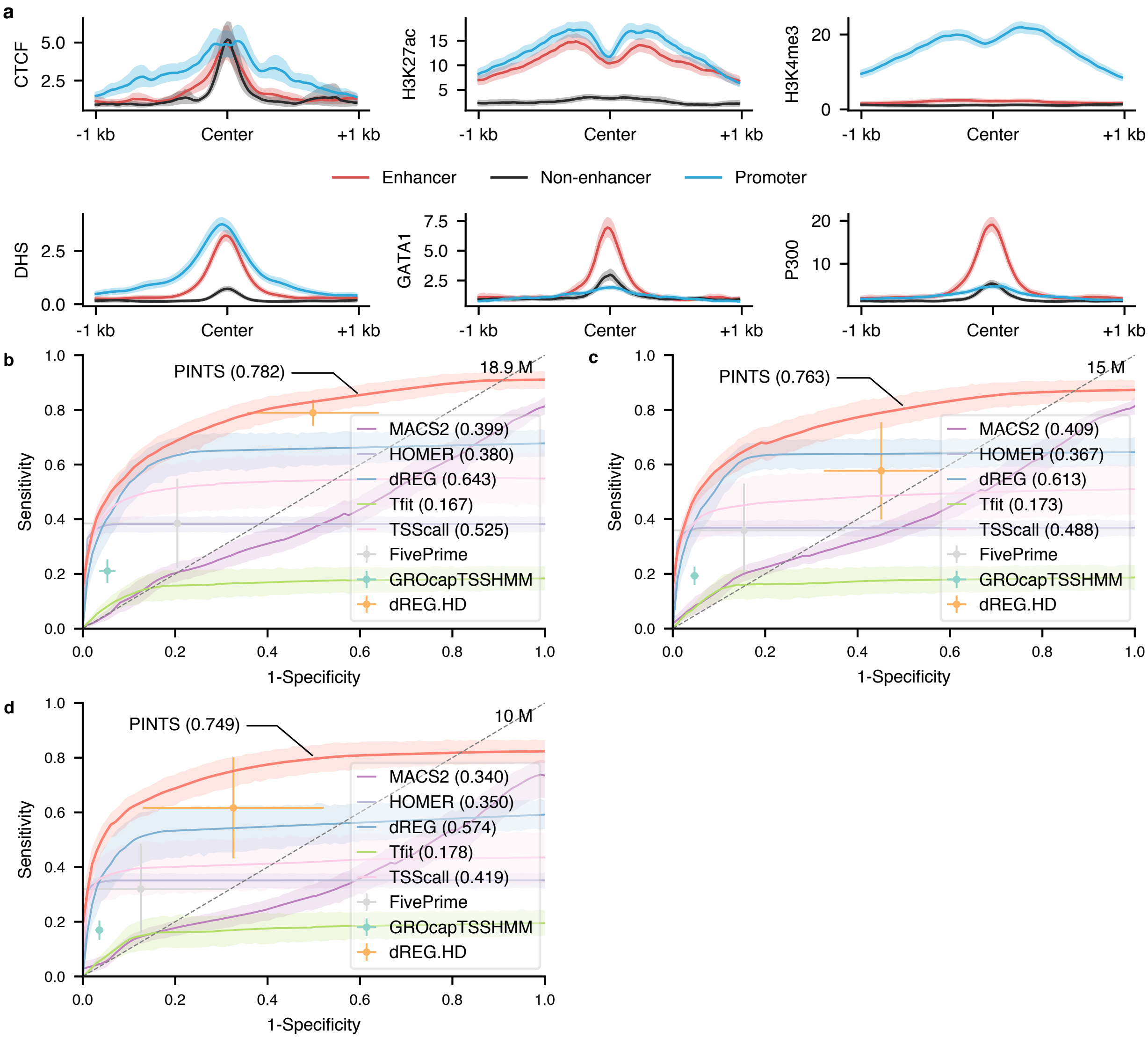

Extended Data Fig. 8 | Performance evaluation of peak callers under different sequencing depths. a, Epigenomic patterns of the true positive (enhancers, promoters) and true negative (non-enhancers) sets used for ROC calculation for peak calling from GRO-cap. **b–d**, Sensitivity and specificity of different peak callers when analyzing TSS-libraries (*n*=7) downsampled to 18.9 (**b**), 15 (**c**), and 10 (**d**) million mappable reads. The corresponding shaded areas show the 95% confidence interval of the means (via bootstrap). For tools where ROCs cannot be calculated, solid dots represent their performance with default parameters. Values and error bars show mean and SD.

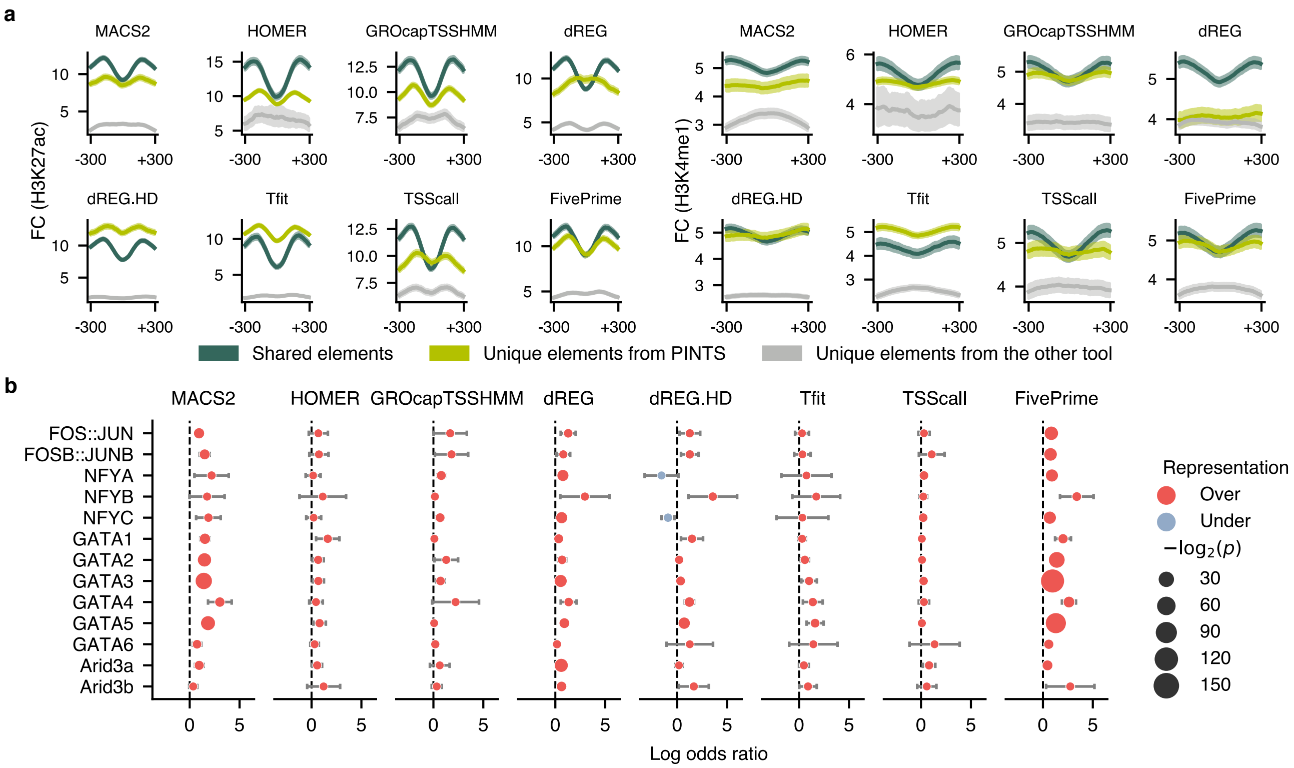

Extended Data Fig. 9 | Profiles of unique distal elements identified by different tools. a, Comparison of the epigenomic signals (fold change over control) in elements uniquely identified by PINTS and other tools. **b**, Enrichment (measured as log odds ratios) of TF-binding motifs in PINTS unique TREs compared to other tools. The circles indicate the corresponding *p*-values ($-\log_2 p$, two-sided *z* tests), and the error bars indicate the 90% confidence interval.

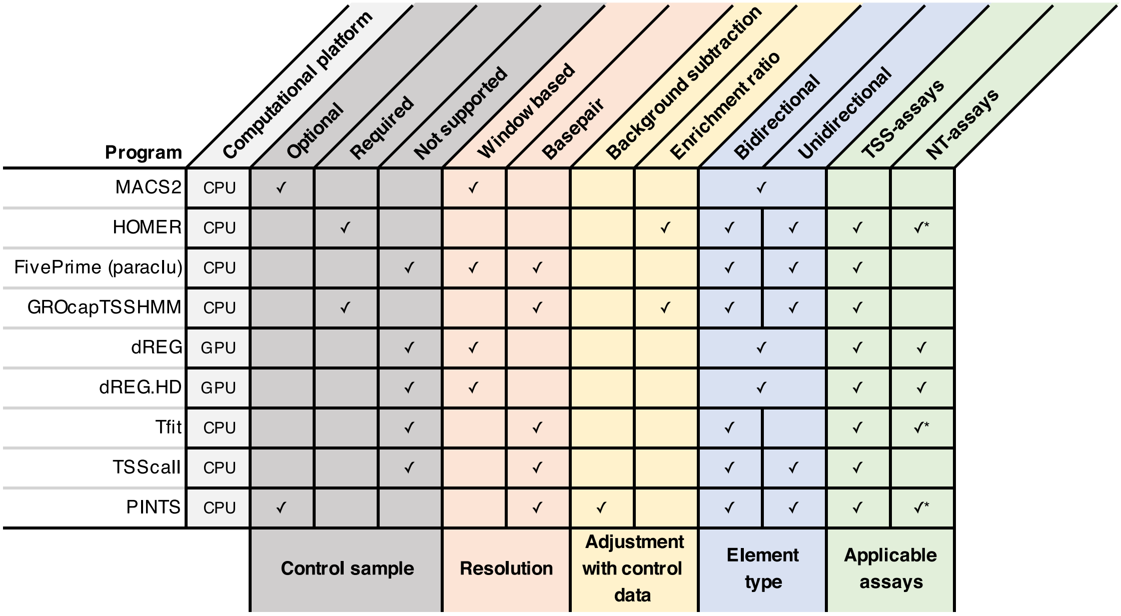

Program	Computational platform	Optional	Required	Not supported	Window based	Basepair	Background subtraction	Enrichment ratio	Bidirectional	Unidirectional	TSS-assays	NT-assays
MACS2	CPU	✓			✓				✓			
HOMER	CPU		✓					✓	✓	✓	✓	✓*
FivePrime (paraclu)	CPU			✓	✓	✓			✓	✓	✓	
GROcapTSSHMM	CPU		✓			✓		✓	✓	✓	✓	
dREG	GPU			✓	✓				✓		✓	✓
dREG.HD	GPU			✓	✓				✓		✓	✓
Tfit	CPU			✓		✓			✓		✓	✓*
TSScall	CPU			✓		✓			✓	✓	✓	
PINTS	CPU	✓				✓	✓		✓	✓	✓	✓*
		Control sample			Resolution		Adjustment with control data		Element type		Applicable assays	

✓*=Not recommanded for Bru- and BruUV-seq.

Extended Data Fig. 10 | A summary of the computational tools compared in this study. The features of different algorithms are summarized and grouped by their roles in the peak calling procedure (colored blocks). Features utilized by each tool to call peaks from nascent transcript sequencing data are indicated.

nature research

Corresponding author(s): John T. Lis and Haiyuan Yu

Last updated by author(s): Jan 3, 2022

Reporting Summary

Nature Research wishes to improve the reproducibility of the work that we publish. This form provides structure for consistency and transparency in reporting. For further information on Nature Research policies, see our Editorial Policies and the Editorial Policy Checklist.

Statistics

For all statistical analyses, confirm that the following items are present in the figure legend, table legend, main text, or Methods section.

n/a	Confirmed	
□	☒	The exact sample size (*n*) for each experimental group/condition, given as a discrete number and unit of measurement
□	☒	A statement on whether measurements were taken from distinct samples or whether the same sample was measured repeatedly
□	☒	The statistical test(s) used AND whether they are one- or two-sided *Only common tests should be described solely by name; describe more complex techniques in the Methods section.*
☒	□	A description of all covariates tested
□	☒	A description of any assumptions or corrections, such as tests of normality and adjustment for multiple comparisons
□	☒	A full description of the statistical parameters including central tendency (e.g. means) or other basic estimates (e.g. regression coefficient) AND variation (e.g. standard deviation) or associated estimates of uncertainty (e.g. confidence intervals)
□	☒	For null hypothesis testing, the test statistic (e.g. *F*, *t*, *r*) with confidence intervals, effect sizes, degrees of freedom and *P* value noted *Give P values as exact values whenever suitable.*
☒	□	For Bayesian analysis, information on the choice of priors and Markov chain Monte Carlo settings
☒	□	For hierarchical and complex designs, identification of the appropriate level for tests and full reporting of outcomes
□	☒	Estimates of effect sizes (e.g. Cohen's *d*, Pearson's *r*), indicating how they were calculated

Our web collection on statistics for biologists contains articles on many of the points above.

Software and code

Policy information about availability of computer code

Data collection

Data were downloaded from NCBI GEO and ENCODE portal via BioQueue (2.0.0).

Data analysis

Data were analyzed using following software tools: BioQueue (2.0.0), fastp (0.20.0), STAR (2.7.1a), samtools (1.11), Picard (2.19.2), Python (2.7.5 & 3.6.9), bedtools (2.29.2), deeptools (multiBamSummary, 3.3.2), numpy (1.19.4), pandas (1.1.4), scipy (1.5.2), statsmodels (0.11.0), pybedtools (0.8.1), pyBigWig (0.3.17), pysam (0.16.0.1), biopython (1.78), MACS2 (2.2.6), HOMER (4.11.1), FivePrime (d39ca4f), GROcapTSSHMM (0.1), dREG (1.4.0), dREG.HD (1.0.1), Tfit (20eb2aa), TSScall (709d2f4), groHMM (1.26.0), STAN (2.20.0), bwa (0.7.17-r1188), Django (3.1.3), bedToBigBed (version 407), bigBedToBed (version 407), bigWigToBedGraph (version 399), bedGraphToBigWig (version 399), bigWigMerge (version 399), liftOver (version 399), JASPAR (version 2020).
The source code of PINTS is freely available at https://github.com/hyulab/PINTS. Analytic pipelines and scripts used to generate results that are reported in this study can be retrieved from https://github.com/hyulab/PINTS_analysis.

For manuscripts utilizing custom algorithms or software that are central to the research but not yet described in published literature, software must be made available to editors and reviewers. We strongly encourage code deposition in a community repository (e.g. GitHub). See the Nature Research guidelines for submitting code & software for further information.

Data

Policy information about availability of data

All manuscripts must include a data availability statement. This statement should provide the following information, where applicable:

- Accession codes, unique identifiers, or web links for publicly available datasets
- A list of figures that have associated raw data
- A description of any restrictions on data availability

Processed TRE calls are publicly accessible via our web portal (https://pints.yulab.org). Data that support the findings of this study are available within the paper and its supplementary information files. All sequencing data analyzed in this study were retrieved from public databases (NCBI GEO and ENCODE portal); lists of accessions are available in Supplementary Tables 1 and 4.

Field-specific reporting

Please select the one below that is the best fit for your research. If you are not sure, read the appropriate sections before making your selection.

☒ Life sciences □ Behavioural & social sciences □ Ecological, evolutionary & environmental sciences

For a reference copy of the document with all sections, see nature.com/documents/nr-reporting-summary-flat.pdf

Life sciences study design

All studies must disclose on these points even when the disclosure is negative.

Sample size	Sample sizes were determined by data availability. No statistical method was used to predetermine sample size. -- We used all available libraries for each of the assays compared in this study.
Data exclusions	No data was excluded from analysis
Replication	Not applicable -- We performed only computational analysis of published data. All available data were used for analyses. Therefore experimental replication is not applicable. The number of repetitions for each analysis (when random subsampling is performed) is provided in the figure legends in the main manuscript and Supplementary Table 1.
Randomization	Not applicable -- no group-wise experimental testing was performed
Blinding	Not applicable -- no group-wise experimental testing was performed

Reporting for specific materials, systems and methods

We require information from authors about some types of materials, experimental systems and methods used in many studies. Here, indicate whether each material, system or method listed is relevant to your study. If you are not sure if a list item applies to your research, read the appropriate section before selecting a response.

Materials & experimental systems

n/a	Involved in the study	
☒	□	Antibodies
☒	□	Eukaryotic cell lines
☒	□	Palaeontology and archaeology
☒	□	Animals and other organisms
☒	□	Human research participants
☒	□	Clinical data
☒	□	Dual use research of concern

Methods

n/a	Involved in the study	
☒	□	ChIP-seq
☒	□	Flow cytometry
☒	□	MRI-based neuroimaging